2006

Fabrication of Oxide Superconducting Thin Films Using Colloid of Nanoparticles as Precursor

Vamsee K. Chintamaneni
Wright State University

FABRICATION OF OXIDE SUPERCONDUCTING THIN FILMS

USING COLLOID OF NANOPARTICLES AS PRECURSOR

A thesis submitted in partial fulfillment
of the requirements for the degree of
Master of Science

By

Vamsee K Chintamaneni
B.Tech., JNTU, 2001

2006
Wright State University

WRIGHT STATE UNIVERSITY

SCHOOL OF GRADUATE STUDIES

07/14/2006

I HEREBY RECOMMEND THAT THE THESIS PREPARED UNDER MY SUPERVISION BY VAMSEE K CHINTAMANENI ENTITLED Fabrication of Superconducting Thin Films using Colloid of Nanoparticles as Precursor BE ACCEPTED IN PARTIAL FULFILLMENT OF THE REQUIREMENTS FOR THE DEGREE OF Master of Science in ENGINEERING

Sharmila M Mukhopadhyay, Ph.D.
Thesis Director

Richard Bethke, Ph.D.
Department Chair

Committee on
Final Examination

Sharmila M Mukhopadhyay, Ph.D.

Suvankar Sengupta, Ph.D.

Raghavan Srinivasan, Ph.D.

Joseph F. Thomas, Jr., Ph.D.
Dean, School of Graduate Studies

ABSTRACT

Chintamaneni, Vamsee Krishna. M.S. Egr., Department of Mechanical and Materials Engineering, Wright State University. *Fabrication of Superconducting thin films using colloid of nanoparticles as precursors.*

This thesis reports the development of a new approach for the fabrication of superconducting oxide thin films. Among the non vacuum liquid phase methods of fabricating high temperature superconductors having critical current density about 1 MA/cm^2, metalorganic deposition using metal trifluoroacetates (TFA-MOD) is the best known method. In this project, detailed spectroscopic and microscopic analysis was performed at every stage of the TFA-MOD process to understand the evolution of crystalline superconducting film. The effect of heating rate on the film properties has been investigated. From these studies it was observed that the TFA-MOD has some inherent disadvantages such as long process time, evolution of HF gas and results porosity in films. A new liquid phase process was developed to fabricate identical superconducting YBCO thin films, which has the potential to overcome the above mentioned drawbacks. This process involves using a precursor, which is a colloidal suspension of Y-Ba-Cu-O nanoparticles of size ~ 20 nm. Precursor films were deposited on LaAlO3 by spin coating or dip coating and heat treated in two stage annealing process to obtain final films. Compared to MOD-TFA processed films, the nanoparticle processed films showed lower porosity and can be grown at faster heating rates. The effect of nanoparticle concentration in colloid, substrate treatment, and solvent on the properties of these films has been reported in this thesis. The superconducting transition temperature (T_c) of nanoparticle processed YBCO films to date is ~ 89 K at R=0. Self-

field critical current densities (J_c) of 2 MA/cm^2 at 77 K have been achieved. These results indicate that this new Nanoparticle method has potential to fabricate long-length, robust YBCO coated conductors.

CONTENTS

LIST OF FIGURES

LIST OF TABLES

Acknowledgement

I owe my most sincere gratitude to my advisor, Professor Sharmila M. Mukhopadhyay, for her immense support, without which I couldn't have come along this far. I would like to express my sincere thanks to Dr. Jianhua Su for his guidance, aid in setting up the experiments and long invaluable discussions we had during the course of project, which had helped to complete my thesis successfully. I would also like to acknowledge Dr. Joshi for his valuable advices and assistance throughout my graduate work.

I would like to thank Dr. Suvankar Sengupta, Dr. Rao Revur and Mr. Troy Pyles for providing me with the sample, colloids and for the project meetings we had, which altogether helped me in carrying out my experiments successfully. I also like to thank Dr. Srinivasan, Dr Mukhopadhyay, and Dr. Jackson for guiding me through my master's work in Material Science at Wright State University. I would also like to thank Greg Wilt for his assistance with analytical instruments in the laboratory.

I would like to thank my friends Kirit Kalagara, Bala Cherukuri, Viswanath Kota, Chaitanya Bandlamudi, Raja Pulikollu, and my sister Lavanya Durgam for their continuous encouragement, invaluable advices throughout my graduate work at Wright State University. I would also like to thank my relatives and other well-wisher for their support.

I am very much indebted to my parents, brothers Anil Chintamaneni, Lalit Chintamaneni and uncle Gopalakrishna Narravula, for their unconditional love, affection, blessings, and continuous support, which made everything possible.

This thesis is dedicated to my parents, Mr. Ch. Nirmalanand,

Mrs. Vijaya, brother Lalit, and uncle N. Gopalakrishna

1. INTRODUCTION

1.1 History

The discovery of superconductivity had created a revolution in science. Its discovery is closely related to that of liquid helium at the University of Leiden by Kamerlingh Onnes in 1908. After this discovery, temperatures as low as 1 K became accessible. In 1911, Onnes found that the electrical resistivity of mercury suddenly dropped to very small values at a temperature of approximately 4.2 K [1]. According to Onnes, "Mercury has passed into a new state, which on account of its extraordinary electrical properties may be called the superconductive state" [2]. Superconductivity was observed in different metals, alloys, and compounds in following years.

1.2 Theory of Superconductivity

A superconductor is a material which loses its electrical resistance below a certain critical transition temperature (T_c) and expels the magnetic field from its interior while below this T_c. This phenomenon of diamagnetism in superconductors is called the MEISSNER effect and was discovered by Meissner and Oschenfeld in 1933. The London brothers proposed a simple theory to explain the Meissner effect in 1935 [4]. According to this, the failure of the diamagnetism in superconductors does not occur abruptly at the surface, but instead the magnetic field penetrates slightly into the bulk of the superconducting material. This penetration depth is called the London penetration depth

(λ) [4] . In 1950 the theory of Landau and Ginzburg described superconductivity in terms of an order parameter (Φ) and provided a derivation for the London equations [5]. Both of these theories were macroscopic.

The first microscopic theory of superconductivity, which is based on electron-phonon interaction, was proposed by American physicists John Bardeen, Leon Cooper, and John Schrieffer in 1957, called BCS theory. According to this theory when an electron travels through a cationic lattice it creates distortion in the lattice (phonons). This creates a greater positive cloud around the electron, which attracts another electron in the lattice. Due to this attractive interaction, electron with opposite momenta and spins form what are known as cooper pairs [6]. The cooper pairs have a slightly lower energy and leave an energy gap above them on the order of 0.001 eV inhibiting the kind of collision interactions which lead to ordinary resistivity. For temperatures such that the thermal energy is less than the band gap, the material exhibits zero resistivity [6]. These cooper pairs are coherent with one another as they pass through the conductor in unison. The correlation distance between the two electrons in the cooper pair is called coherence length (ζ) [7].

1.3 Types of Superconductors

Superconductors can be classified in to two groups, Type I and Type II based on their magnetic and current carrying properties.

1.3.1 Type I superconductors

Type I superconductors, also called soft superconductors, are mostly comprised of metals and metalloids. These are well modeled by BCS theory. They completely expel magnetic flux from their interior with the help of the surface currents. Figure 1.1 shows the graph of induced magnetic field of a Type I superconductor versus applied field. When an external magnetic field is applied to a Type I superconductor the induced magnetic field exactly cancels that applied field until there is an abrupt change from the superconducting state to the normal state. Type I superconductors have only one very low critical magnetic field (H_c) [4]. Hence the practical applications of these superconductors are not feasible.

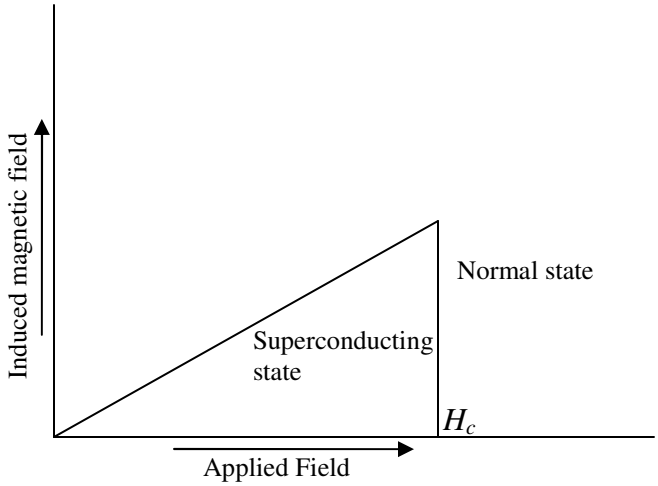

Figure 1.1: Graph of induced magnetic field of a Type I superconductor versus applied field

1.3.2 Type II Superconductors

Type II superconductors, also called hard superconductors, are mostly comprised of metallic alloys and compounds. Figure 1.2 shows a graph of the induced magnetic fields of a Type II superconductor versus the applied field. Below the lower critical field (H_{c1}), the superconductor excludes all magnetic field lines. At field strengths between H_{c1} and the higher critical temperature (H_{c2}), the magnetic flux partially penetrates into the material. When this occurs, the material is said to be in the **mixed state** [4]. In this region some of the areas shift to normal regions so that it can accommodate the flux line of the field. Above H_{c2} the material returns to its normal state.

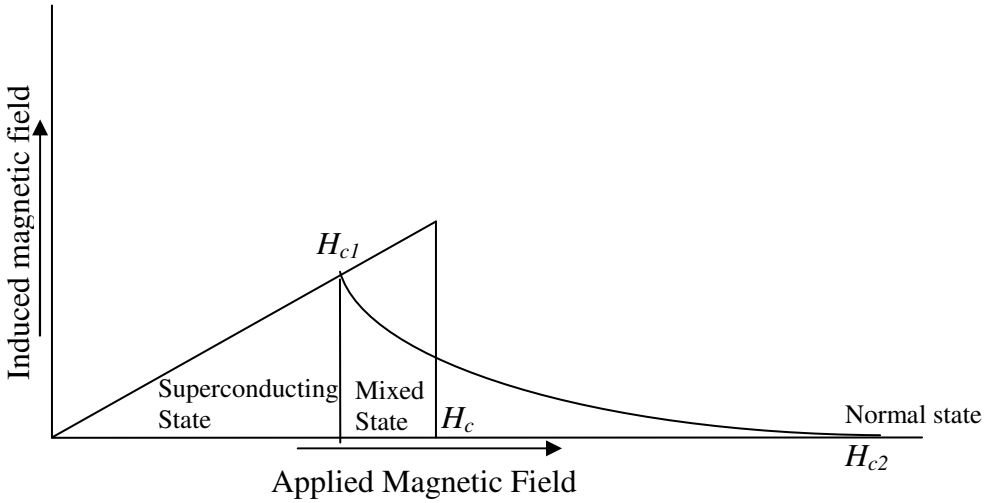

Figure 1.2: Graph of induced magnetic field of a Type II superconductor versus applied field

1.3.3 High Temperature Superconductors (HTS)

Three decades after BCS superconductors, a startling discovery reopened the field of superconductivity research. In 1986 at IBM in Switzerland, Bednorz and Müller discovered a new class of superconducting materials LaBaCuO (30 K) [8]. The following year, $YBa_2Cu_3O_{7-x}$ (YBCO) was discovered, which is superconducting at 90 K. showing a scope for use of superconductors at liquid nitrogen temperature (77 K). In the following years many superconductors were developed which had T_c above liquid nitrogen temperature. Notable among these were the Bi-Sr-Cu-O with T_c = 85 K [9] , Bi-Sr-Ca-Cu-O with T_c = 115 K [10] , Tl-Ca-Ba-Cu-O with T_c = 125 K [11] and Hg-Ba- Ca-Cu-O with T_c= 135 K [12]. All these superconductors have copper oxide planes. Hence these are also known as cuprates or copper oxide superconductors. Of the four types of cuprates YBCO has the most potential for HTS applications. The performance of YBCO thin films in the presence of magnetic fields is far superior to bismuth based superconductors, due to the higher irreversibility line [13]. The irreversibility fields for $Bi_2Sr_2Ca_2Cu_3O_x$ (Bi - 2223) and YBCO is illustrated in Fig. 1.3 [13] . Thallium and mercury based superconductors have higher T_c than YBCO, but they are not as attractive due to their toxic nature.

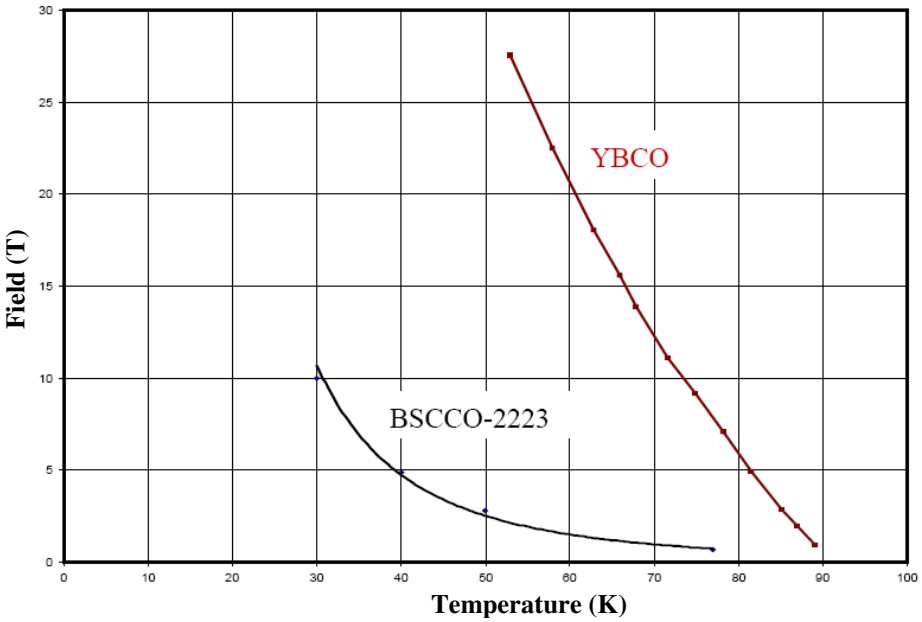

Figure 1.3: Irreversibility fields for Bi-2223 and YBCO [13]

1.4 YBCO Crystal Structure

All high-T_c superconductors are related to pervoskites with layered structure, in which the presence of CuO_2 layers plays a determinant role in their superconducting character. The carriers only move along these planes, while the other components act as charge reservoirs that regulate the charge density in the CuO_2 planes. In the case of YBCO, each unit cell contains two CuO_2 superconducting planes, separated by a plane of yttrium atoms, all sandwiched by two BaO layers, as shown in Fig. 1.4. The compound can present two possible symmetries, tetragonal or orthorhombic, depending on the amount and distribution of oxygen in the final Cu-O layers (charge reservoir) which close the cell. In the formula $YBa_2Cu_3O_{7-x}$, if x is close to zero we have orthorhombic structure, which is superconducting. When x>0.5 we have tetragonal structure. The lattice

parameters for superconducting YBCO are: a = 3.8227 Å, b = 3.8872 Å, c = 11.6820 Å [15]. The layered structured in YBCO leads to anisotropic behavior in this HTS material The conductivity along a-b planes is greater than that along c- direction, *i.e* $J_c^{ab} >> J_c^{c}$. Hence a c-axis oriented structure is needed for high-power applications [16].

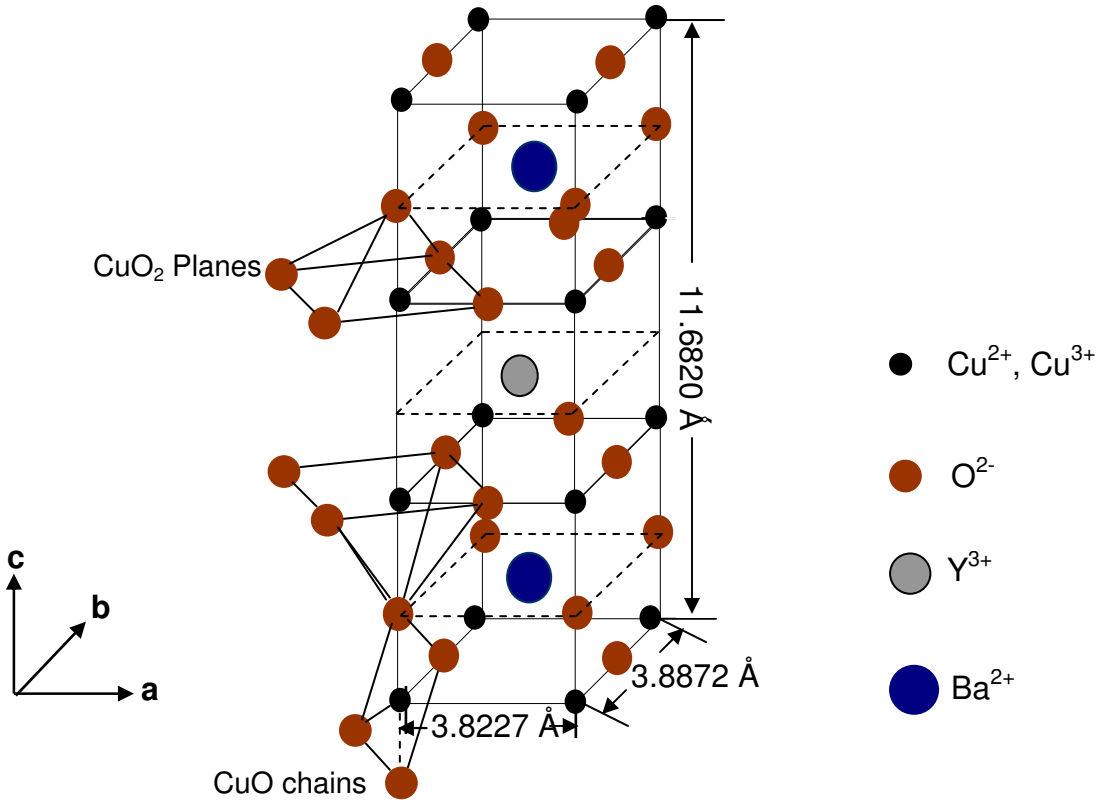

Figure 1.4: Schematic view of crystal structure YBCO showing CuO_2 planes and CuO chains [14]

1.5 YBCO Thin Films:

After the discovery of superconductivity in YBCO it was realized that, however bulk sintered ceramic, which are weakly coupled across the grain boundary, could not carry current more than that of copper, single crystal YBCO thin films showed high $J_{c,}$ at 77 K [17]. This was due to high angled grain boundary in case of bulk and polycrystalline substrate when compared to thin films [18]. It was found that the upper limit for grain misorientation for good J_c is ~ 5° [19] . Very high critical current densities, ($J_c > 10^6$ at 77 K) can be achieved in thin films, making YBCO a promising material in the future for high power applications. However, preparation of these thin films with desired qualities is a challenging problem for every processing method as discussed in the following section.

1.5.1 Architecture of Coated Conductor

The HTS coated conductor to be used as second generation wire consists of a thin flat metal foil or polycrystalline metal on top of which a buffer layer is deposited, over which the epitaxial YBCO thin film is grown followed by the final silver layer as shown in Fig. 1.5 . There are two main approaches to attain long length coated conductors with high critical current densities. The first one is deposition of biaxial textured buffer layers on a polycrystalline metal substrate using deposition techniques such as ion beam assisted deposition (IBAD) [20] or incline substrate deposition (ISD) [21]. The second method involves first the fabrication of biaxial textured metal surface using rolling assisted

biaxially textured substrate (RABiTS) method, followed by the deposition of epitaxial buffer layer which gets the biaxial texture of the substrate. The buffer layer principal functions are: (i) to provide epitaxial growth of YBCO layer and (ii) act as barrier for chemical diffusion between superconducting layer and the substrate. The final superconducting layer can be grown using different techniques, which will be discussed in the following section.

Figure 1.5: Typical architecture of YBCO coated conductors [19]

1.5.2 Fabrication of YBCO Thin films

The fabrication techniques used to make the final YBCO layer can be broadly classified into two classes, in-situ and ex-situ. In the case of in-situ, crystallization of oxides occurs during deposition on a heated substrate where as in ex-situ nucleation and growth occur during post-deposition heat treatment. Both of these methods are capable of producing thin films with good transport properties.

In-situ film growth techniques like pulsed laser deposition (PLD), molecular beam epitaxy (MBE), thermal co-evaporation and sputtering have been successfully used for the synthesis of epitaxial YBCO [19]. Among these vacuum based methods, the PLD technique developed by Los Alamos National Laboratories (LANL) [19] and University of Goettingen in Germany [24] is widely used. In this method, YBCO targets are vaporized or ablated by a laser source; these vapors are then deposited onto a substrate at about 800 ^{o}C in a low pressure atmosphere containing $O_2 - N_2$ mixture [25]. Since PLD method involves transfer of YBCO from a target source to the substrate surface, the stoichiometry of the target can be preserved in these films. These films have excellent compositional homogeneity [27]. J_c values higher than 1 MA/cm^2 at 77K were observed in films fabricated by this method with high reproducibility [28]. The cost of scaling up is a challenge for this approach, which includes the cost of lasers, tubes, windows, gases, high-vacuum systems and HTS targets. A lower vacuum and potentially low cost technique called Metal Organic Chemical Vapor Deposition (MOCVD) was developed by Fujikura [29] and IGC superpower [29]. In this method, a volatile precursor compound is evaporated and carried to a heated substrate using a carrier gas, where the film growth occurs due to chemical reactions at the substrate surface [31]. The commonly used precursor compounds are $Y(TMHD)_3$, $Ba(TMHD)_2$, $Cu(TMHD)_2$ where TMHD stands for 2,2,6,6-tetramethyl-3-5 Heptanedionate or β – diketonate. These compounds are mixed in an organic solvent that consists of tetrathydrofuran (THF), isopropanol and tetraglyme to form the final precursor solution. The application of this precursor coating is carried out at temperatures between 600 - 800 ^{o}C using a nitrogen carrier gas [25]. Deposition rates as high as 150 Å/s have been obtained by this method with J_c~ 1

MA/cm^2 [32]. The deposition area in this method is limited by the area of the showerhead, which is unlimited [30]. This technique too has some challenges including (i) uniformity in the film over larger areas (ii) the cost incurred for the complex raw materials to prepare the precursor (iii) film composition due to its sensitivity to substrate temperature and (iii) equipment cost.

Liquid phase techniques could be an alternative to vapor phase approaches due to the simplicity of the deposition process, vacuum less procedure, efficient use of all precursor material, and the relatively low cost of the furnaces needed to react the precursor to the superconducting state [13]. One of the liquid phase techniques, metalorganic deposition (MOD) process holds great potential as a method of fabricating YBCO thin films. It is a fast and efficient method of producing large-scale, biaxially-textured superconducting films at lower cost than physical and chemical vapor deposition techniques [33]. However, in most MOD processes except one, J_c over 1 MA/cm^2 (77 K, self-field) is seen rarely in these films [[32]. The poor transport properties are attributed to the stability of $BaCO_3$ which forms as an intermediate compound during decomposition of carboxylates [33]. The MOD process using Metal trifluoroacetate (TFA) precursors is an exception. This approach avoids the formation of $BaCO_3$ during decomposition. Initial investigation of TFA-MOD process was conducted by Gupta *et al.* in 1988 [34]. Afterwards, McIntyre *et al.* first reported high J_c (> 1 MA/cm^2) for YBCO film using the TFA-MOD process [35]. This is an effective method of producing large-scale, bi-axially textured superconducting films at lower cost than any other method to-date [36]. However, it has some inherent drawbacks [37]: (i) it needs a very careful

optimization of heating rates, and very long processing times are needed and (ii) it releases highly corrosive HF during processing which is not only an environmental concern, but also the cause of significant porosity in the final film. It will therefore be beneficial to investigate an alternative liquid phase approach that can fabricate films of these oxides without the drawbacks listed above. To start with nanoscale particles containing the constituent ions (Y-Ba-Cu-O) may be an attractive option. By starting with oxides of cations rather than fluoroacetates, gaseous by-products could be significantly reduced or completely eliminated. Nanoscale particles having higher surface area are expected to crystallize more easily at lower temperatures and at faster rates. We have developed a new method in collaboration with Metamateria Partners LLC, a company in Columbus that specializes in nanoscale processing of oxides. This new synthesis route called Nanoparticle process use the colloidal dispersion of Y-Ba-Cu-O nanoparticles as precursors.

The second approach *i.e.* fabrication of YBCO films using nanoparticle of Y-Ba-Cu-O in a colloid form, was developed by our group and no prior publication exists in the literature. The first approach (TFA-MOD) has been developed over the last few years and current state of knowledge in this field has been discussed in the following section.

1.5.3 TFA-MOD Process

Gupta et al. [34] have first introduced TFA-MOD method for the fabrication of YBCO thin films. The idea of using metal trifluoroacetates originated from studies of

Mankiewich et al. [38], where they successfully used BaF_2 in place of other Ba compound for fabrication of superconducting thin films using co-evaporation technique. Textured YBCO with sharp transition of T_c (R=0) = 94 K was reported by Gupta et al. [34] using this method. Several years later in 1991, McIntyre and Cima reported critical current densities over 1MA/cm^2 with T_c above 90 K [35]. Since then many research groups have reported high J_c's on single crystal and metal buffered substrates [42].

In the TFA-MOD method, the precursor solution is obtained by reacting aqueous solution of metal (Y, Ba and Cu) acetates with stoichiometric quantities of trifluoroacetic acid (TFA), then drying followed by mixing with methanol. The precursor is light blue in color before mixing with methanol, after which it turns deep blue. The blue color is mostly from the copper ions. The substrates can be either spin coated or dip coated to obtain a gel film. The gel film is calcined at 400 ^oC in humid oxygen atmosphere for long periods to get the precursor film. It mainly involves the decomposition of metalorganic salts to oxyfluoride intermediate states. These chemical reactions results in > 50% decrease in thickness and an increase in the internal stresses of the films. In order to avoid the cracking in the film due to these stresses a very slow calcining profile has to be used (~20 hrs). During the calcining process the fluorine replaces oxygen linked to Y and Ba as it very electronegative, whereas carbon cannot replace oxygen hence it is expelled. The calcined films are fired at 800 ^oC in a humid furnace atmosphere, where the intermediate films are converted to crystalline, superconductive Y123 films.

Several groups have investigated the complex reactions during the calcining and firing stages [41-44]. Gupta et al have reported that all the metal trifluoroacetates decompose around 300 ^{o}C in argon atmosphere. The weight loss and high temperature x-ray analysis has shown yttrium and barium trifluoroacetates decompose to respective fluorides, YF_3, BaF_2 and whereas copper trifluoroacetate forms a mixture of CuO, Cu_2O, CuF_2 [34]. Smith et al. [44] has reported the intermediate compounds of $Y_2Cu_2O_5$, BaF_2, and CuO after calcination using high temperature x-ray study and fluorine removal study. Araki et al. [43] reported that the precursor mainly consists of CuO nanocrystallite and amorphous matrix of Y-Ba-O-F or Y-Ba-Cu-O-F using TEM energy dispersive x-ray spectroscopy. The pyrolysis mainly occurs in the temperature zone of 250–300 ^{o}C. TGA/DTA analysis has shown that exothermic reactions occur during this period and most of the weight loss and shrinkage occurs during this stage [45]. . McIntyre et al. [35] reported that Cu in the gel film sublimes as copper trifluoroacetate when the humidity is low during the calcining process. Araki et al. [36] has observed the same thing using TG-DTA results. The average size of CuO nanocrystallites in a precursor grows during heating between 200 – 250 ^{o}C in the calcining process creating localized inhomogeneities in the composition of the film [45]. The grain growth of these CuO nanocrystallites can be decreased by increasing the humidity in the firing process. The overall reaction that occurs during crystallization can be represented by the following equation [44]

$$½Y_2Cu_2O_5 + 2BaF_2 + 2CuO + 2H_2O \rightarrow YBa_2Cu_3O_{6.5} + 4HF.$$

Humidified argon gas mixed with 50-500 ppm oxygen gas is used to remove the fluorine from the film. To understand the firing process, Araki *et al* [42] defined a quasi-liquid consisting of Y, Ba, Cu, O, H, and F, which exits for certain atomic composition. YBCO grains precipitate out from this liquid onto a lattice matched substrate surface while releasing HF gas. The reaction has to be precisely controlled to get the epitaxial nucleation of $YBa_2Cu_3O_{6.5}$. The HF removal from the surface of these film limits the growth of the YBCO grains [45]. Tokunaga et al. [48] claimed that the removal of HF from the film results in a macroporous film. The film is oxygenated at 450 °C for couple of hours to transform non-superconducting tetragonal YBCO to superconducting orthorhombic YBCO superconductor. The conversion of precursor film to final film results in > 50% reduction in thickness of the film causing further pores and shrinkage at this stage.

Though high J_c films have been fabricated with good reproducibility using this method, there are some challenges associated with it: (i) the long processing time required to burn out the organics during the calcining process (ii) high porosity in the final film due to the gases evolved during the whole process of fabrication (iii) evolution of highly corrosive HF gas during the firing and handling of this gas during large-scale processing is a big problem and (iv) difficulty in fabrication of thick YBCO films (2-5 μm) without considerable decrease in J_c. The first two problems may be addressed if we have a fundamental understanding of the chemical reactions during calcining and firing process. Although there are many studies on the chemical reaction and growth mechanisms using thermal techniques, several aspects of it still are not understood [44],

[46]. X-ray Photoelectron Spectroscope (XPS) can be used to study chemical reactions that occur during calcining and firing of the film. No reports on x-ray photoelectron spectroscopy (XPS) investigation for the TFA-MOD process have been reported to date. A systematic study on the effect of heating rate during the calcining process on the microstructure, surface chemistry and electrical properties would be helpful in having an understanding to control the microstructure and film properties on these superconducting films. This study has been done by this group.

An approach using nanoparticles of yttrium, barium, copper cations as starting raw material has been developed in collaboration with Metamateria LLC a company in Columbus that specializes in nanoscale processing of oxides. This process may result in lower porosity as gaseous by-products can be significantly reduced, and it is expected that the use of nanoparticles might lower the processing temperature and time. This method has been termed as nanoparticle method in this thesis.

1.6 Objective of the Thesis

The work of this thesis is divided into two tasks.

Task 1: To have fundamental understanding of the TFA-MOD process. Spectroscopic and microscopic analysis will be performed in conjunction with electrical properties measurement in order to study the changes going on during the calcining and firing process in the TFA-MOD method. The effect of heating rate during the calcining on final film properties will also be studied.

Task 2: To develop an alternate method to the TFA-MOD process. Nanoparticle of Y-Ba-Cu-O in a colloid form will be used as precursor solution. A process has to be developed form a dense, epitaxial film using nanoparticle precursor solution. The properties of these Nanoparticle processed film will be compared to that that of TFA-MOD processed sample.

2. EXPERIMENTAL PROCEDURES

This chapter gives a detailed description of sample fabrication using the TFA-MOD and Nanoparticle methods as these are the main techniques which have been used in thesis work. The characterization techniques used throughout this thesis are also discussed briefly.

2.1 TFA-MOD Method

2.1.1 Substrate Preparation

Lanthanum aluminate was used in this study due to its close lattice match with the YBCO crystal. 10 mm x 10 mm x 0.5 mm, (100) oriented, single-side polished lanthanum aluminate (LAO) single crystal substrates were obtained from Coating and Crystal Technology. The substrates were sliced into small pieces with dimensions of 5 mm x 10 mm using a diamond stylus. These substrates have been cleaned before they were used for film fabrication. A three step cleaning procedure is followed as it is very critical in getting good films. The substrates were first ultrasonicated in chloroform for 15 minutes followed by ultrasonication in acetone for 15min and finally ultrasonication in methanol

Before dip coating or spin coating these cleaned substrates were checked with the optical microscope to make sure that the surface was spot free.

2.1.2 Synthesis of Precursor Solution

A typical synthesis process for preparation of the precursor solution is given in figure 2.1. Acetates of yttrium, barium and copper are mixed in the molar ratio of 1:2:3.05 in deionized water using a glass rod. A stoichiometric quantity of TFA is added to this solution and mixed using a magnetic stirrer until all the acetates have dissolved into the solution. The solution thus obtained is dried overnight at 125^{o} C in a box type furnace to obtain a glassy blue gel residue. The residue is dissolved in sufficient methanol to give a cationic solution with concentration of 1.0M. The color of this solution is a deep blue from the Cu^{2+} ions. When this solution is left alone over-night, a thick residue is observed at the bottom of the beaker. Care has been taken such that only the clear solution is transferred from the beaker and used for experiments. The solution thus obtained seems to have very long shelf life time in a closed bottle at room temperature.

2.1.2 Precursor Coating

Deposition of the TFA precursor onto the single crystal substrate can be done using a variety of techniques used for industrial film-coating processes. The processes which are being considered for commercialization are dip coating and slot die casting. In this

thesis, the samples were prepared mostly by dip coating. In very few cases spin coating was used. The description of the dip coating method is given in figure 2.2.

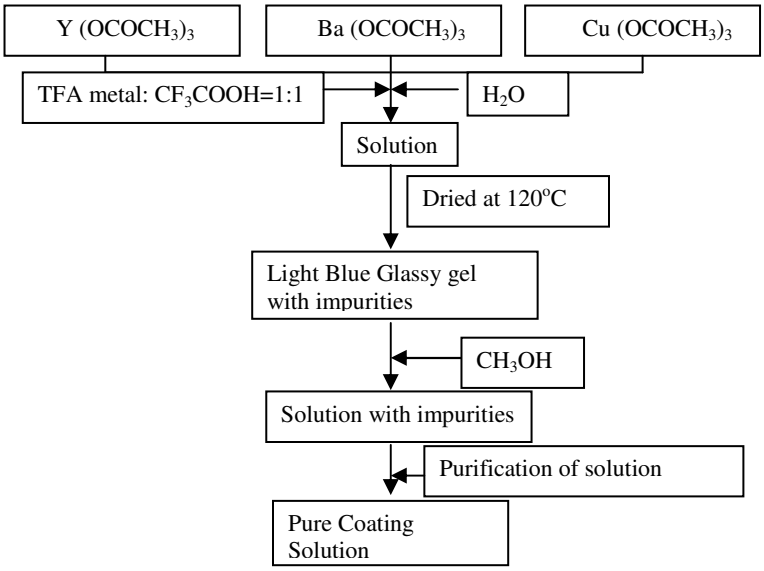

Figure 2.1: Process for preparing the Precursor coating solution [37]

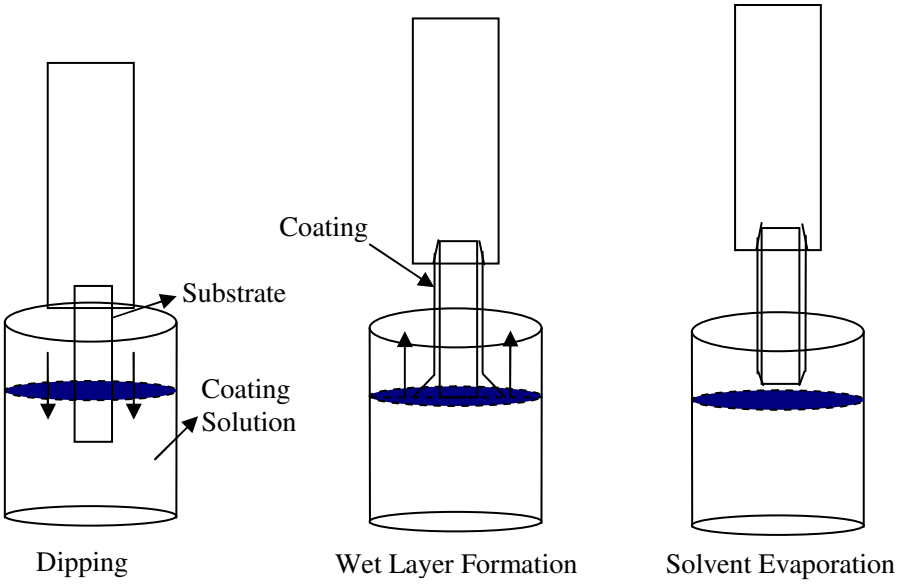

Figure 2.2: Dip Coating Process for preparing the Precursor film

2.1.3 Calcination of the Precursor Film

Calcination of the precursor film is needed to decompose the metal organics and burn out the impurities in the precursor to result in a film containing Yttrium, Barium and Copper compounds.

Calcination of the as-deposited film is done in a mullite horizontal tube furnace. The experimental setup for this process is shown in figure 2.3. The sample is placed 2-3 cm from the center in the horizontal mullite tube, as the homogenous temperature zone is within this range. The temperature of the sample is monitored by a K-type thermocouple mounted along the centerline of the furnace with its tip located above the sample. The humidified gas required during the process is obtained by passing the gas through de-ionized water contained in three 500 mL conical flasks which are arranged in series as shown in figure 2.3. Care was taken to prevent the release of HF vapors in air by purging the outgoing gas through de-ionized water and exhausting into the hood.

The heating program during this process was optimized by our group, details of which are given elsewhere [37]. The optimized heating profile is given in figure 2.4. The heating profile was programmed using a Eurotherm temperature controller. Dry oxygen was used until 110^{o} C to avoid water absorption into the sample. The gas flow rate was controlled at 2 L/min through out the process using a gas flow meter. Humid oxygen gas was used in the process to suppress the sublimation of copper oxide. After the furnace reaches 400^{o} C, gas flow is stopped and the sample is furnace cooled. Typically the

sample is removed from the furnace when the temperature is less than 100^{o} C. and the calcined film looks light brown in color.

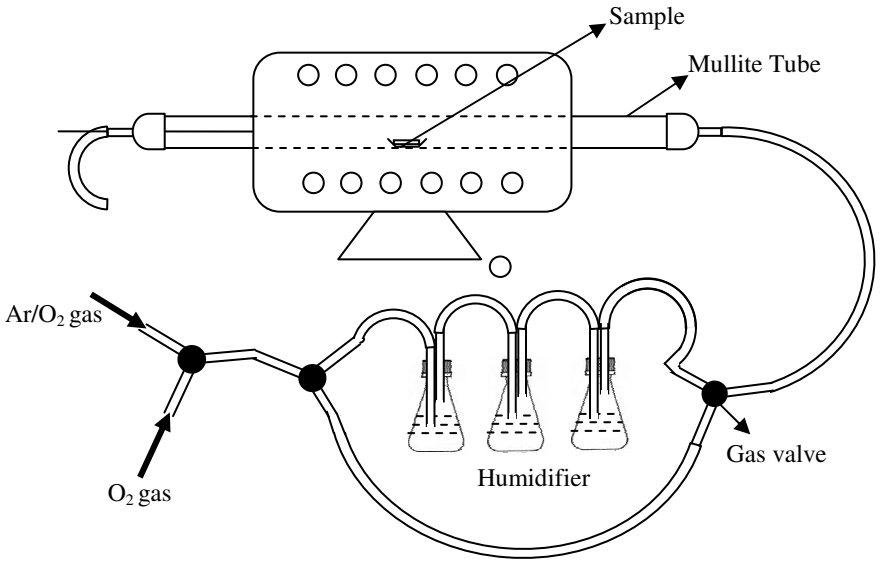

Figure 2.3: Experimental Setup for the fabrication of YBCO superconductor

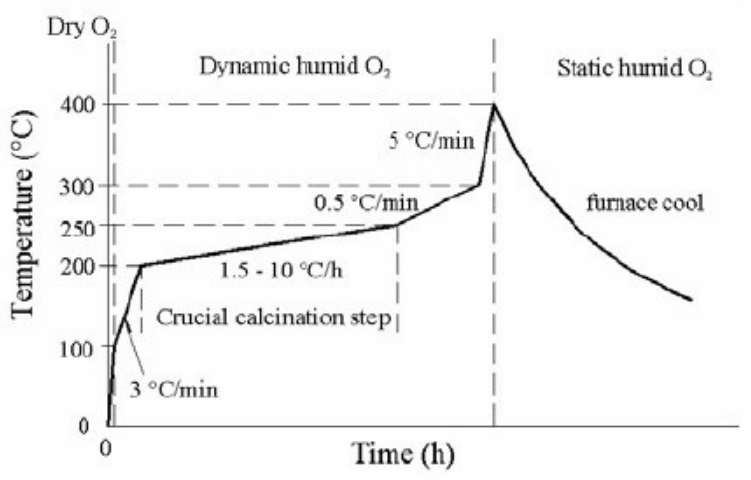

Figure 2.4: Heating Profile for Calcination of the TFA-MOD film [37]

2.1.4 Firing of the Film

The calcined film is fired at 800° C in humid atmosphere with low oxygen vapor pressure. An Ar/O_2 mixture with 200ppm of O_2 is used here. The firing program used in this study is given in figure 2.5. During the heat treatment, a mixture of dry Ar/O_2 gas was used until 400° C to avoid the condensation of moisture inside the furnace near the sample. After that, a humid Ar/O_2 mixture was used until 800° C. The flow rate is maintained at 2L/min using the gas flow meter throughout the process. An earlier publication indicates that humid gas is used to convert metal oxyfluoride to oxides [46]. The furnace was maintained at 800° C for 60 minutes for the conversion of fluorides to oxides and subsequent growth of YBCO. The furnace is slowly cooled to 450° C at a rate of 3° C/min in dry Ar/O_2 mixture until 525° C and thereafter by dry O_2 gas. The sample was annealed in the dry O_2 atmosphere at 450° C for 90 min to convert non-superconducting tetragonal YBCO to superconducting orthorhombic YBCO. After the program is completed, the furnace was switched off, gas flow was turned off and the sample was furnace cooled to room temperature. The final film should be black and shiny.

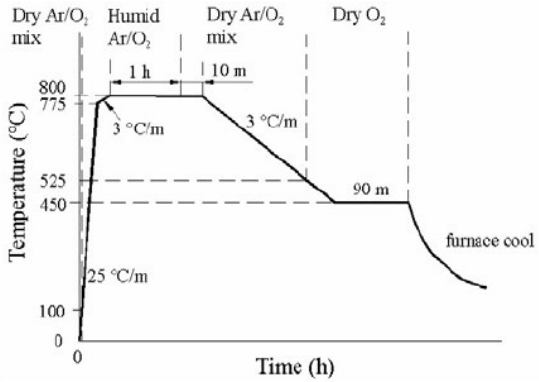

Figure 2.5: Heating Profile for Firing of the TFA-MOD film [37]

2.2 Fabrication using Nanoparticle Method

This approach is completely initiated by our group and no prior publications exist to use as a starting platform. Therefore, optimization and trials for this method were little more challenging. The procedures for this method are outlined in the following sections.

2.2.2 YBCO Nanoparticle Synthesis

Colloids containing YBCO nanoparticles were used as precursors. These were obtained from a Metamateria Partners LLC (our collaborator in this project). Nanoparticles containing Y, Ba, Cu and O are prepared by using an organometallic decomposition route (Fig. 2.6).

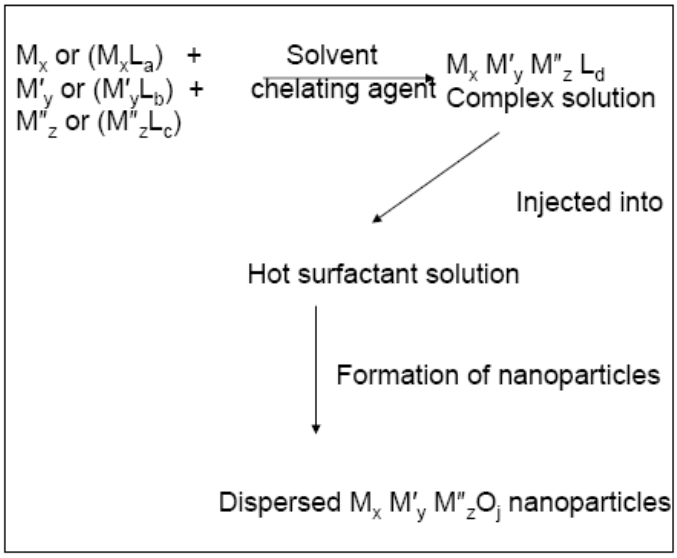

Figure 2.6: Synthesis of YBCO nanoparticles using the organometallic decomposition method

The color of the colloid varied from dark green to blue depending on the concentration. The size of the nanoparticles obtained viewed by AFM showed was < 20 nm which is shown in Fig.2.7and 2.8.

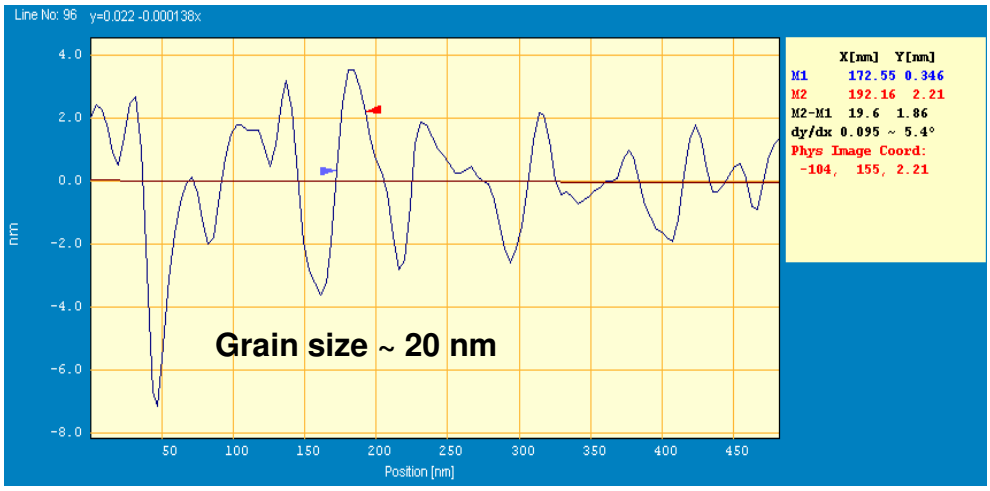

Figure 2.7 : AFM Line scan generated on a particular area on ybco nanoparticle film.

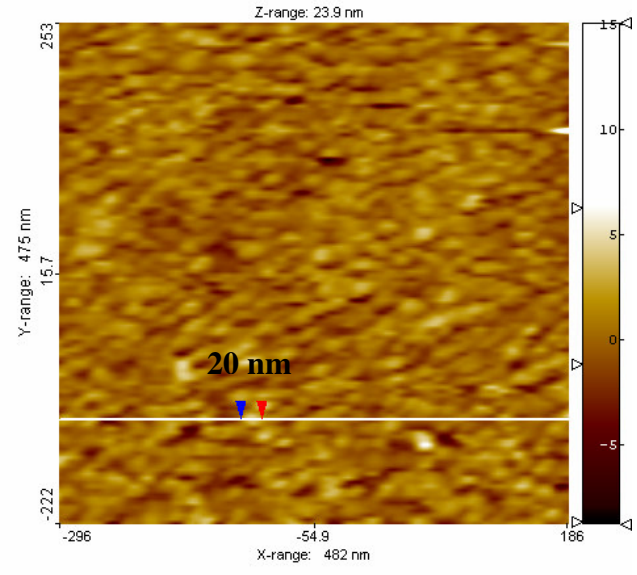

Figure 2.8: AFM analysis on film fired till 400 ^{o}C (Courtesy Dr Xioming Hu, WSU)

Coatings were applied on LAO either by dip coating or spin coating. Dip coating is similar to that discussed in section 2.1.3. Spin coating is done on a custom made spin coater. The sample is held firmly at the centre of the spin coater with help of double stick tape. The whole set-up is kept in the hood in order to avoid contamination on the film. The spin coating speed is fixed at 3600rpm. The spinning time depends on the desired thickness and viscosity of the colloids. The typical spinning time varies from 2 - 3 minutes.

2.2.3 Heat Treatment

The as-prepared film is subjected to two separate heat treatments in horizontal mullite tube furnace as shown in Fig. 2.3. The experimental setup for this heat treatment is similar to that of TFA-MOD heat treatment (Fig. 2.3), but the rate of the first heat treatment is much higher. This is one of the expected advantages of this approach and will be elaborated later.

During the first stage of heat treatment, the sample is subjected to 400^{o} C temperature following the heating program given in Fig. 2.9. In this program a slower ramp rate from 200^{o} C to 300^{o} C was used as it was observed from DTA measurements that around 250^{o} C there was an exothermic reaction which also resulted in major weight loss. It is believed that the weight loss is mostly due to evaporation of the 1, 4 butanediol solvent. The sample was heated till 110^{o} C in dry O_2 in order to avoid condensation of water vapor. Humid O_2 was used there after till 400^{o} C to avoid copper oxide sublimation

and to prevent the loss of film integrity. The flow rate of gas was maintained at 2 L/min throughout the process. After the temperature of the furnace reaches 400^{o} C, gas flow is switched off and the furnace is left to cool down to room temperature. The film is taken out and checked for its uniformity and defects, if present. The total heat treatment time is less than 6 hr as compared to the 20hrs of calcination in the TFA process.

The second heat treatment profile is same as that is used by TFA firing process. A detailed description of this process was given in sec 2.1.4.

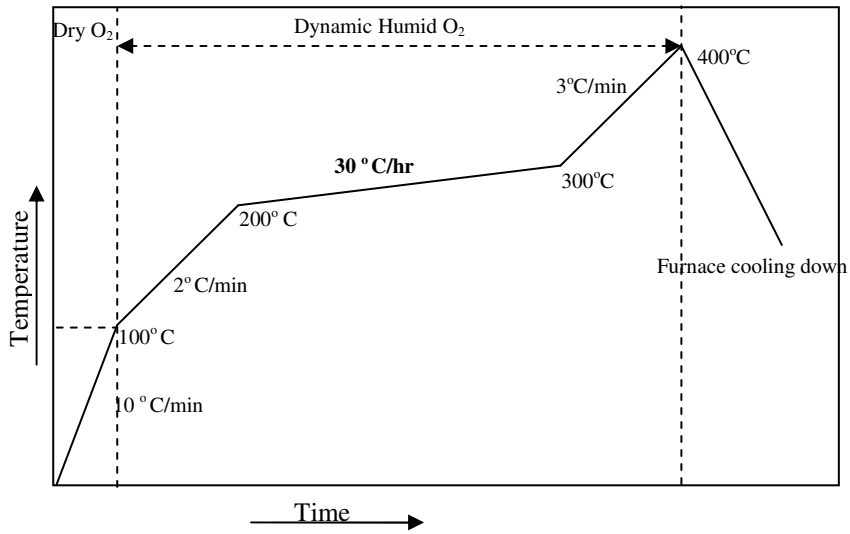

Figure 2.9: First stage heating profile for the Nanoparticle process. Note that the slower heating rate step (200 ^{o}C – 300 ^{o}C) in this case is 60 times less than that in figure 2.6.

The texturing of the film was characterized using XRD and Surface morphology was studied using SEM. The chemistry and electrical properties of the samples was studied using XPS and four point dc current-voltage method respectively.

2.3 Characterization Techniques

Different characterization techniques were used in this study. X-ray Photoelectron Spectroscopy (XPS) was used to study the surface chemistry, x-ray Diffraction (XRD) was used to study the crystallographic orientation, Scanning Electron Microscopy was used to study the surface morphology and Four-point method was used to study the electrical properties of the films. A brief introduction of these techniques is given below.

2.3.1 X-ray Photoelectron Spectroscopy (XPS)

XPS not only identifies the element present on the top few atomic layers but also indicates their chemical bonding states; hence it has been used in this study for studying the chemistry of the samples. The basic working principle of XPS is depicted in figure 2.10. In this process a photon of known energy interacts with the sample surface causing in ejection of electron from it, the kinetic energy of this outgoing electron is by related to the original binding energy of that particular electron by the equation given below.

$$E_K = h\nu - E_B$$

where, E_K= Kinetic Energy

E_B= Binding Energy

$h\nu$ = Photon Energy

The binding energy of a particular electron is its characteristic property and therefore the measurement of kinetic energy of that particular photoelectron will enable the identification of the elements. These photoelectrons are detected by an electron spectrometer. The analyzer is normally operated as energy “window”, accepting only the

electron having energy within the range of this fixed window (pass energy). The electrons are detected as discrete events and the number of electrons for a given detection energy and time is stored digitally [49].

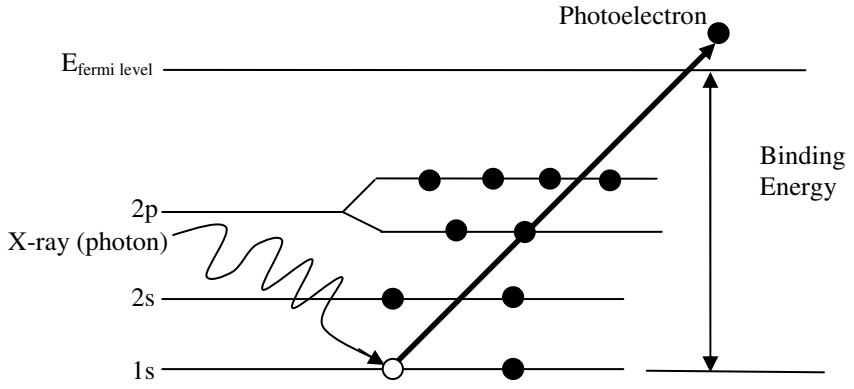

Figure 2.10: Photoelectric Effect in XPS

All the XPS experiments during this study were done using an AXIS ULTRA from KRATOS ANALYTICAL Inc (Figure 2.11). Monochromatic Aluminum X-rays are used as the photon source in this instrument. The system consists of two chambers: sample transfer chamber (STC) and sample analysis chamber (SAC), which are separated by a gate valve. The sample is mounted on a stub using a double stick carbon tape. The mounted sample is first introduced into STC and left there until the pressure in that chamber reaches 1 x 10^{-7} Torr. The gate valve is opened to transfer the sample from STC to SAC. The typical pressure in the SAC is around 10^{-9} Torr. A charge balance of 2.62 V was kept for charge neutralization. A high voltage of 14 KV and current of 10 mA is applied on the filament to produce the required X-rays. The analyzer was operated with

the entrance slot placed and fixed pass energy of 40 eV. An 8-channeltron multi-detector was used to amplify and record the signal. Analysis on the sample is averaged on 110µm x 110µm area. A plot of electron pulses versus the analyzer energy range gives the photoelectron spectrum, which is then stored into a UNIX based computer. The obtained spectrum was processed using vision 2.0 software.

In most of the cases the samples need to be cleaned to remove the contamination from the top surface. The sample is etched by 3 KeV Ar^+ ion bombardments using an ion gun. The pressure is maintained at 3 x 10^{-8} Torr in SAC during the etching process. The spot size of the ion beam is 650µ.

Figure 2.11: XPS AXIS ULTRA from KRATOS ANALYTICAL Inc. (funded by NSF and OBR)

2.3.2 Scanning Electron Microscope (SEM)

Scanning electron microscopy is a commonly used technique in the material characterization. A focused electron beam is rastered over the sample surface; due the interaction of this electron beam and the sample surface several emissions are observed [50]. Among these secondary electrons and back scattered electrons are used to form the image on the cathode ray tube by mapping the intensity of the detected signal as a function of the position of the incident beam .

Scanning Electron Microscope used in this study is a JOEL 35-CF (fig 2.12). Typical operating voltage is 15 kV. Secondary electron images were obtained keeping the working distance at around 15 mm to get a better image. No sample preparation was done. There is an Energy Dispersive X-ray Diffraction (EDX) attached to the SEM to get the elemental information. The SEM was used to check the grain structure, grain orientation, porosity, secondary phases, and film homogeneity. Cross-sectional SEM provided the estimate of the thickness of the deposited film.

Figure 2.12: JSM 35-CF Scanning Electron Microscope from JOEL USA Inc

2.3.3 X-Ray Diffraction (XRD)

XRD is a widely used technique for the crystal structure analysis and for the identification of secondary phase in the sample. The basic working of XRD is governed by Bragg's law. Bragg's law assumes that crystals are built up in layers or planes and are spaced at a distance 'd' apart. When an X-ray is incident on these planes, they diffract or reflect, and these reflected rays interfere constructively if they satisfy the Bragg's law.

$$2d \text{ Sin } \theta = n\lambda \text{ [50]}$$

Where θ is the angle of incidence of X-rays, λ is the wavelength of X-rays, n is the order number of the reflection. From the values of θ, λ, and n the value of d is obtained and we can obtain the crystal orientation from these 'd' values. The schematic diffractometer geometry is show in fig 2.13.

Philips PW 1830 XRD was used in these studies. Cu K_α having a wavelength of 1.5418 generated by applying 45 kV and 35 mA on the source are used as the X-ray source. X-rays are diffracted from the sample and by varying the angle of incidence of X-rays a diffraction pattern is obtained that is characteristic of the sample. The diffraction pattern peaks are identified with an internationally recognized database. No sample preparation is required in this case.

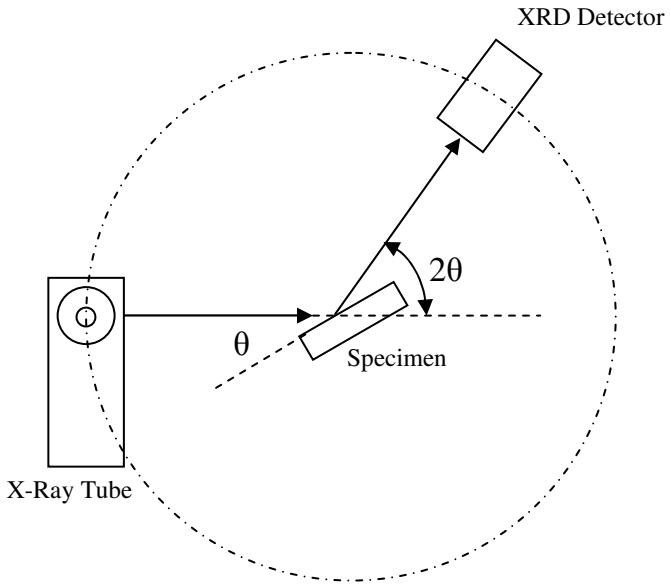

Figure 2.13: Principle of an X-ray Diffractometer

2.3.4 Measurement of Superconducting Properties

The superconducting properties, critical current(I_c) and critical temperature (T_c) of the specimen are measured using the four point probe method. A schematic diagram of the four point probe with the sample is shown in Fig. 2.14. Indium wire is used at the edges of the specimen for better contact with the copper plates. The probe is immersed in liquid nitrogen. In the case of measurement of critical temperature (T_c), liquid nitrogen is slowly evaporated and the change in voltage with respect to temperature is acquired. A LabVIEW program is used to convert this data to get a final plot of Resistance Vs Temperature, which gives the value of T_c. In the case of measurement of critical current the temperature is kept constant and the current is varied, voltage is plotted against the

current to get the critical current. The current is increased at 0.1 A per step during the measurement of I_c. 1 μV/cm criterion is used to determine I_c. The distance between the voltage taps is 3 mm, 4 mm for T_c and I_c measurements respectively. The transport critical density of the sample was calculated by dividing the I_c by the cross-sectional area of the sample, which is measured using a microscope.

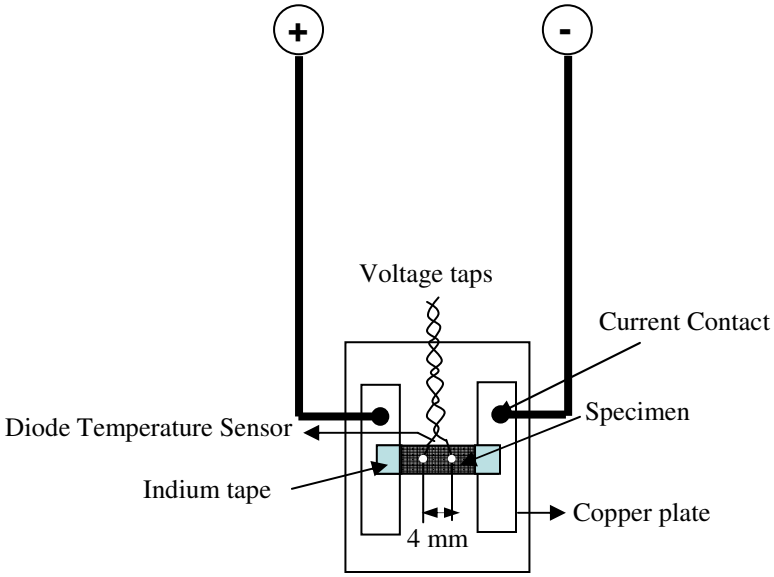

Figure 2.14: Illustration of the four point probe for the measurement of transport properties

3. RESULTS AND DISCUSSION

3.1 Fundamental Studies to understand the Evolution of YBCO from Metallic TFA Precursors

3.1.1 XPS Studies on TFA – MOD Process

XPS analysis was done on samples at every step of the calcining and firing processes so as to have a fundamental understanding of the chemical reactions that occur as the precursor evolves to a crystalline superconducting film.

Figure 3.1 shows the comparison of C 1s XPS spectra obtained on the films before and after the calcining process. Before calcination, the C 1s has several components. The component occurring at 292.5 eV is due to the $–CF_3$ group, while the one at 289.2 eV is –COOH. After calcining process these two components become weak, indicating decomposition of fluoroacetates group during calcination. The third component of C 1s peak is observed at 284.7 eV on films both before and after calcination and can be attributed to the C-O-R and/or the atmospheric contaminants absorbed during sample transfer. Figure 3.2 shows the F 1s spectra obtained on the films before and after calcination. The F 1*s* spectra for the samples before calcination have two components, a high binding energy at ~ 687.9.0 eV representing the CF_3 bonds and a low

binding energy at 684.5 eV, which can represent either BaF_2 or CuF_2. It has been reported by various groups [49, 51, 52] that the binding energy of BaF_2 ranges from 683.7 to 684.2 eV and CuF_2 [49] ranges from 684.3 to 685.9 eV. However, the 684.5 eV peak is not attributed to CuF_2 as Cu $2p_{3/2}$ peak does not indicate any presence of Cu-F bonds. Hence that peak has been attributed to BaF_2. After calcining there is only a single peak at 684.1 eV which represents Ba-F.

Figure 3.3a shows the Y 3d spectra before and after calcination. For a film after calcination, the binding energy of the Y $3d_{3/2}$ peak is 158.0 eV, which less than that of YF_3 (159 eV) [51], [54], [55], but greater than that of Y_2O_3 (156.5 eV) [49, 51]. Araki *et al.* has reported the formation of amorphous YOF compound during calcination [36]. So we assumed that 158 eV peak represents oxy-fluoride of Y^{3+} ion. This is further supported by earlier study by Rizhkov et al [55] where a binding energy of 157.6 eV was reported for a Y-O-F component, which is close to that measured in this instrument. Moreover, F in Y-O-F has a reported binding energy of 685.3 eV [55], which could be within the envelope of the larger BaF_2 peak. Figure 3.3b shows the Ba 3d peak for films before calcination and after calcination. The Ba 3*d* XPS spectra shows a strong peak at 780.6 eV for the film before calcination which is representative of Ba $(CF_3COO)_2$. The Ba $3d_{5/2}$ peak at 779.8 eV in case of calcined sample has been associated with BaF_2.

XPS analysis was done on samples at the early stage of firing (after the sample reaches 800^{o} C) and after firing. Figure 3.4a and b shows the Ba 3d, F 1s peaks for these films respectively. The Ba $3d_{5/2}$ XPS spectra for samples in early stages of firing shows a

peak at 779.8, associated to BaF_2 while the fired sample peak is at 778.5 which is attributed to BaO in an YBCO structure. The F 1s peak for the case of sample in the early stage of firing represents the BaF_2. As the film is fired this peak diminishes. This indicates that after firing, all the fluorine is eliminated leaving a textured YBCO film.

In summary it has been observed from these XPS experiments that all the acetates and fluorocarbon groups were removed after calcination process. The calcined film mainly consists of Y, Ba, Cu, O, and F, where Yttrium is present as Y-O-F, Barium is presents as BaF_2, and Copper is in form of CuO. During the early stages of firing, Barium is still in fluoride form but after firing all the fluorine is eliminated as HF gas leaving Barium in oxide form in the final film.

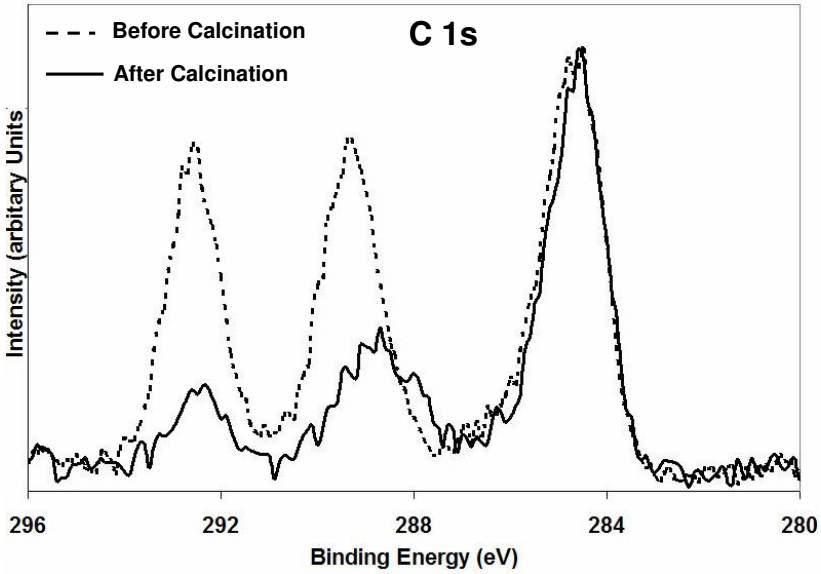

Figure 3.1: XPS spectra of C 1s obtained on the films before and after calcination.

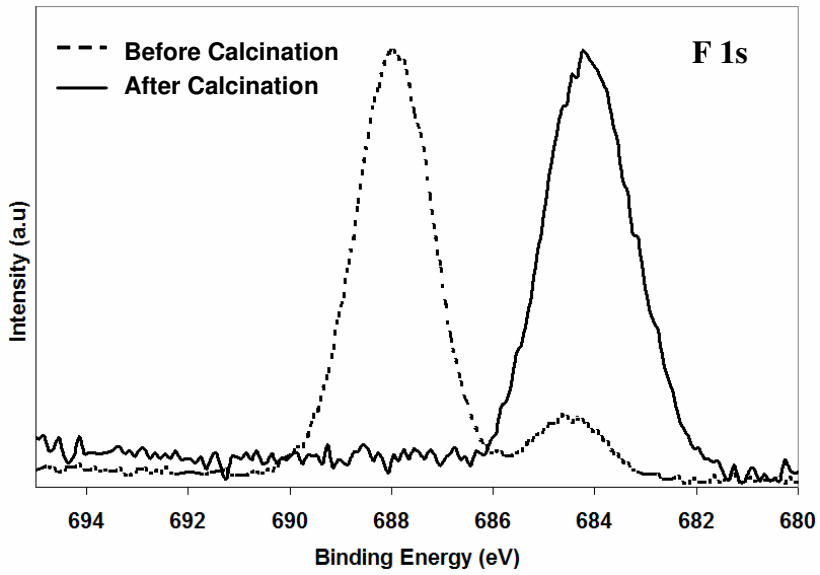

Figure 3.2: XPS spectra of F 1s obtained on the films before and after calcination.

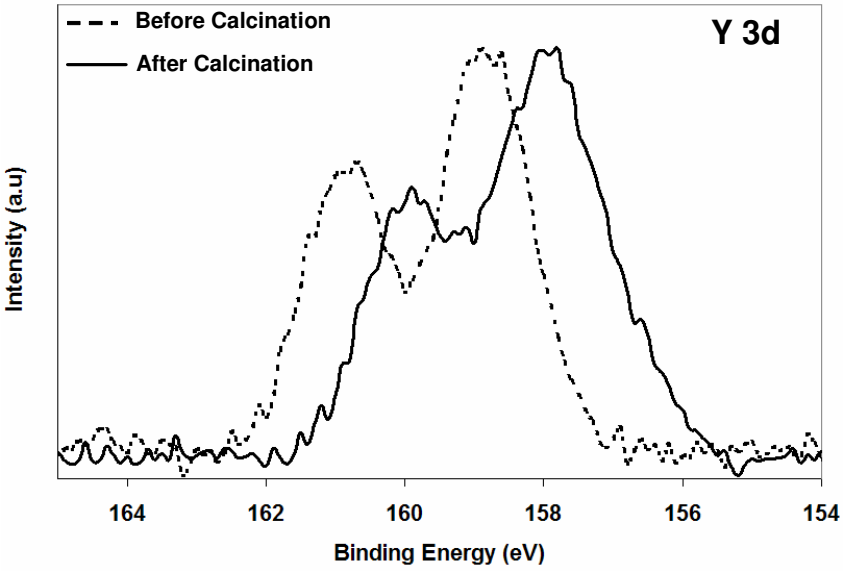

Figure 3.3a: XPS spectra of Y 3d obtained on the films before and after calcination.

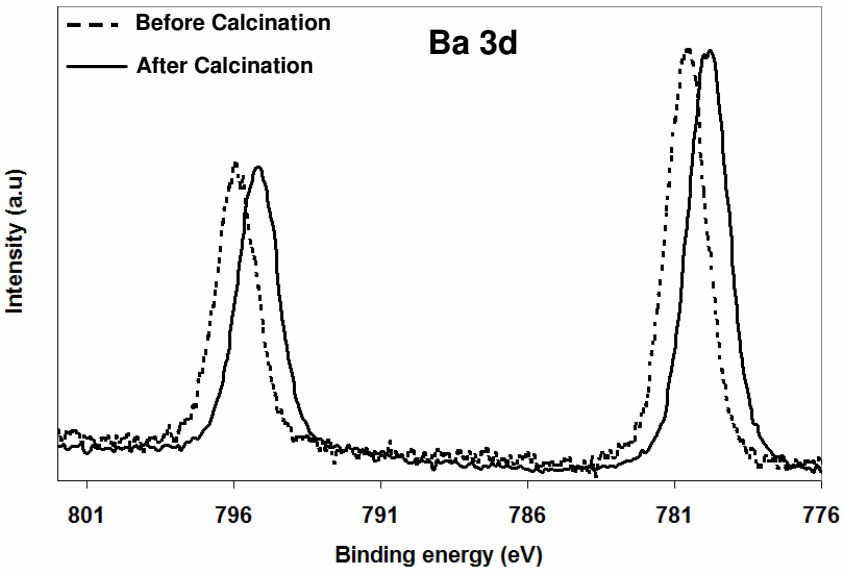

Figure 3.3b: XPS spectra of Ba 3d obtained on the films before and after calcination.

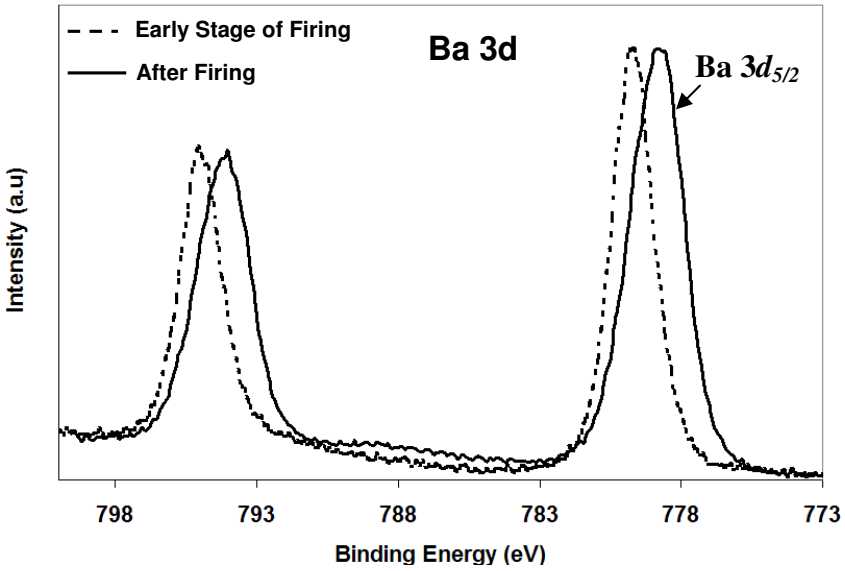

Figure 3.4a: XPS spectra of Ba 3d obtained on the films early stages of firing and after firing.

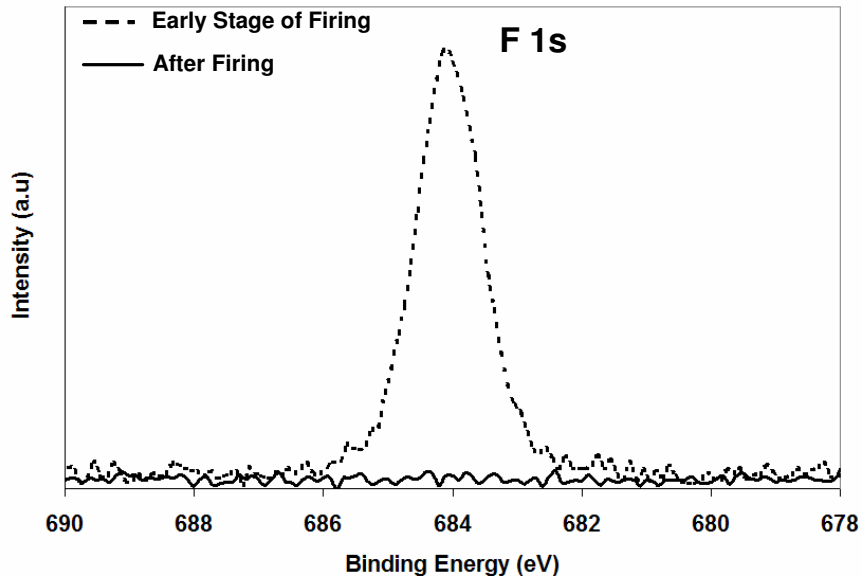

Figure 3.4b: XPS spectra of F 1s obtained on the films early stages of firing and after firing.

3.1.2 Effect of Heating Rate on Films Fabricated using TFA-MOD Method

The removal of organics is a crucial step during the first treatment of the film. Two parameters which were found to have influence on this are heating rate and atmosphere. The effect of calcination heating rate on the microstructure and electrical property of the final film has been investigated. It has been reported that the most critical step during the calcination is the 200 ^{o}C – 250 ^{o}C step [35, 46]. Three different heating rates, 1.5 ^{o}C/hr, 3 ^{o}C/hr and 10 ^{o}C/hr were used during this step to study the effect of it on film properties and in turn optimize the TFA – MOD method.

XPS analysis was done on all three samples and it was observed that the heating rate did not change the overall chemistry of the films (Fig. 3.5). The surface

morphologies of the calcined films heat treated at 1.5 ^{o}C/hr, 3 ^{o}C/hr, and 10 ^{o}C/hr are shown in Fig 3.6a,b and c respectively. The films calcined at the slowest rate (1.5 ^{o}C/h) have a granular surface (Fig. 3.6a). It was reported that most of the Cu in the precursor films converts into CuO nanocrystallites during the calcination process [36]. So when a slower heating rate (1.5 ^{o}C/hr) was used CuO crystallites had sufficient time to separate out as a second phase, which can be observed from the micrograph (Fig 3.6a). In case of the intermediate heating rate (3 ^{o}C/hr), a smooth and uniform surface was obtained (Fig. 3.6b). The film calcined at 10 ^{o}C/h showed an uneven surface with porous features (Fig. 3.6c), possibly due to rapid the escape of HF gas.

These calcined films were fired to 800 ^{o}C following the heating profile given in Fig. 2.5. Surface morphologies of fired films are shown in Fig. 3.7a, b, and c. Figure 3.7a shows the microstructure of the fired film which was calcined at 1.5 ^{o}C/hr. The surface has lot of a-axis oriented grains which can characterized by the presence of columnar or needle like structure. Large white particles are also observed which were found to be copper rich zones. The microstructure observed in the case of 3 ^{o}C/h heated films was smooth, uniform, and c-axis oriented (Fig. 3.7b). In case of the faster calcined sample no *a*-axis oriented grains were observed (Fig. 3.7c), however these films had bigger pore size and high pore density when compared to that of 3 ^{o}C/h calcined sample. Critical temperature was measured on all three samples. The T_c's at R=0 (~ 88 K) were found to be same for all the three samples (Fig. 3.8). When critical current densities were measured on all three samples it was found that the 3 ^{o}C/hr treated sample had the highest

J_c of 1.3 MA/cm^2. XRD of this 3 ^{o}C/hr treated final film shows that the film obtained is c-axis textured (Fig. 3.9).

The influence of heating rate during the calcining process on film chemistry, microstructure, and electrical properties has been investigated. It can be seen that the heating rate does not change the overall chemistry of calcined films. Surface morphology of the calcined films depends on heating rate. The 3 ^{o}C/hr calcined film resulted in a uniform, smooth calcined film and well textured final YBCO film. Heating rates had no significant effect on critical transition temperature (T_c), however critical current density (J_c) was found to be higher for 3 ^{o}C /hr treated sample. The total process time for the optimized TFA-MOD is 28 Hrs. There is significant porosity observed in the final YBCO films. The critical current density, J_c = 1.3MA/cm^2 and critical temperature, T_c = 88.5 K were observed in this optimized film.

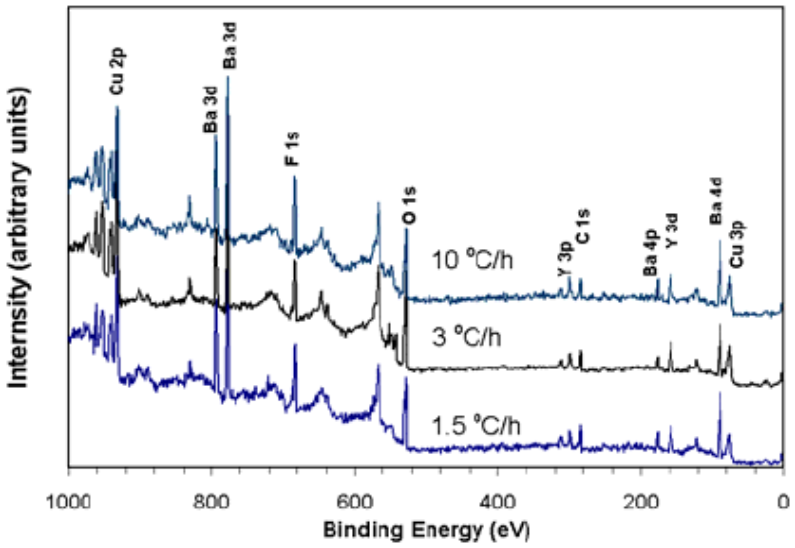

Figure 3.5 XPS survey scan for calcined films heated at different rate

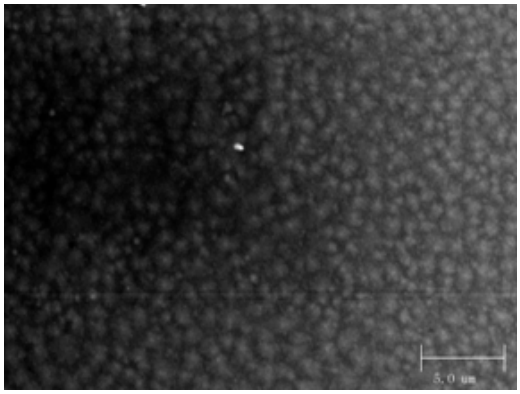

Figure 3.6a: Microstructure of calcined sample heated at 1.5 ^{o}C/hr during the 200 – 300^{o}C step.

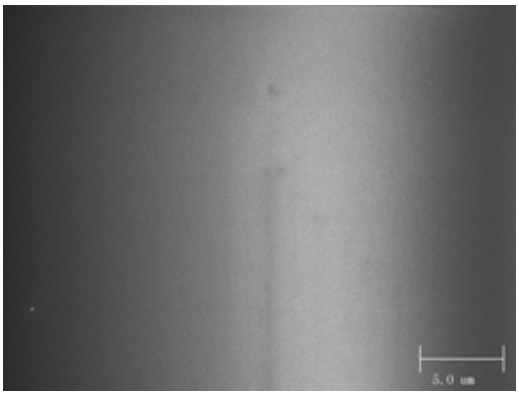

Figure 3.6b: Microstructure of calcined sample heated at 3 ^{o}C/hr during the 200 – 300^{o}C step.

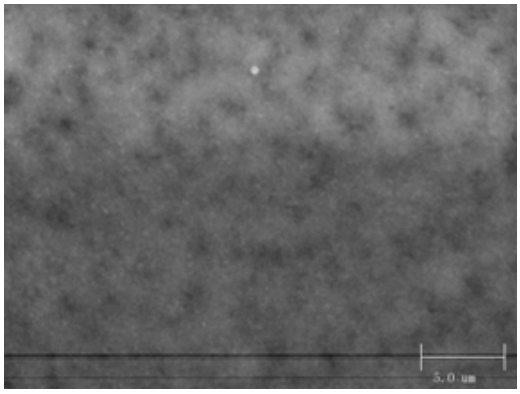

Figure 3.6c: Microstructure of calcined sample heated at 10 ^{o}C/hr during the 200 – 300 ^{o}C step.

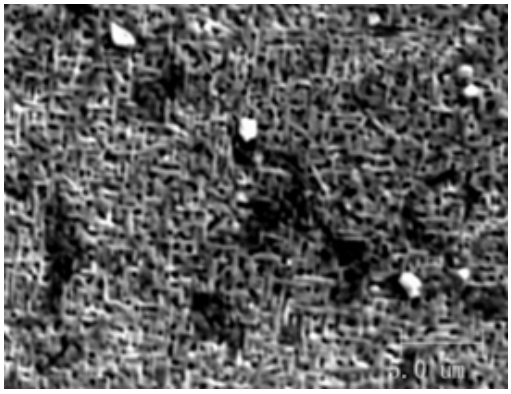

Figure 3.7a: Microstructure of calcined sample heated at 1.5 ^{o}C/hr during the 200 – 300 ^{o}C step.

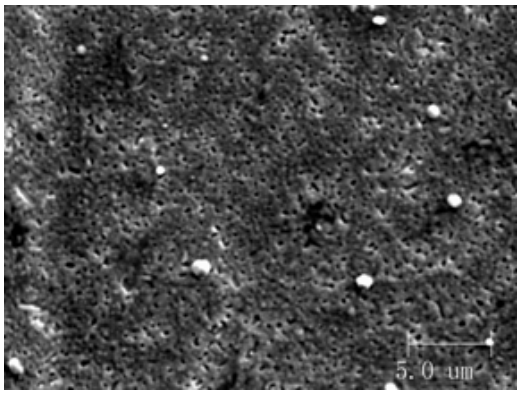

Figure 3.7b: Microstructure of calcined sample heated at 3 ^{o}C/hr during the 200 – 300 ^{o}C step.

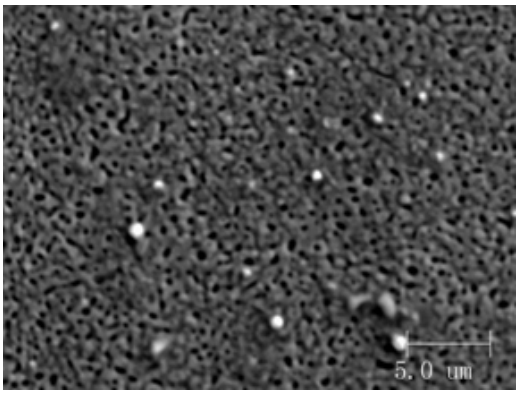

Figure 3.7c: Microstructure of calcined sample heated at 10 ^{o}C/hr during the 200 – 300 ^{o}C step.

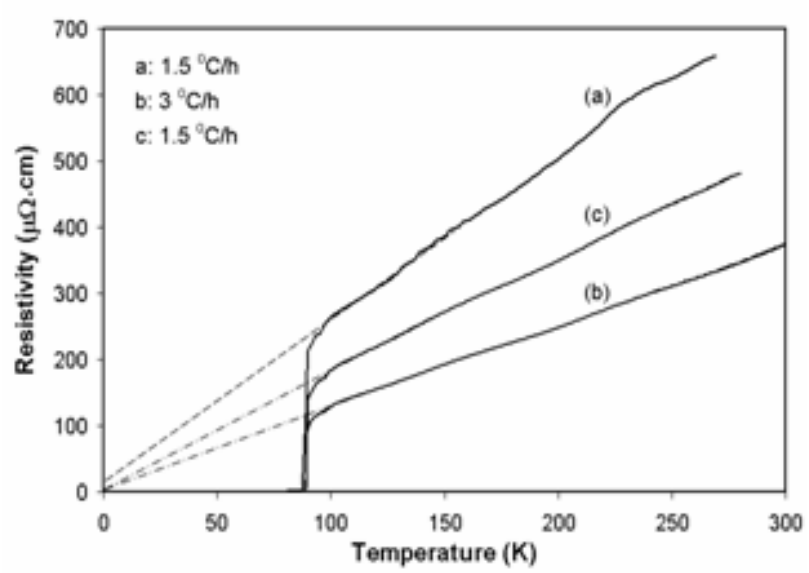

Figure 3.8: Temperature dependence of the electrical resistivity for YBCO films calcined at different heating rates.

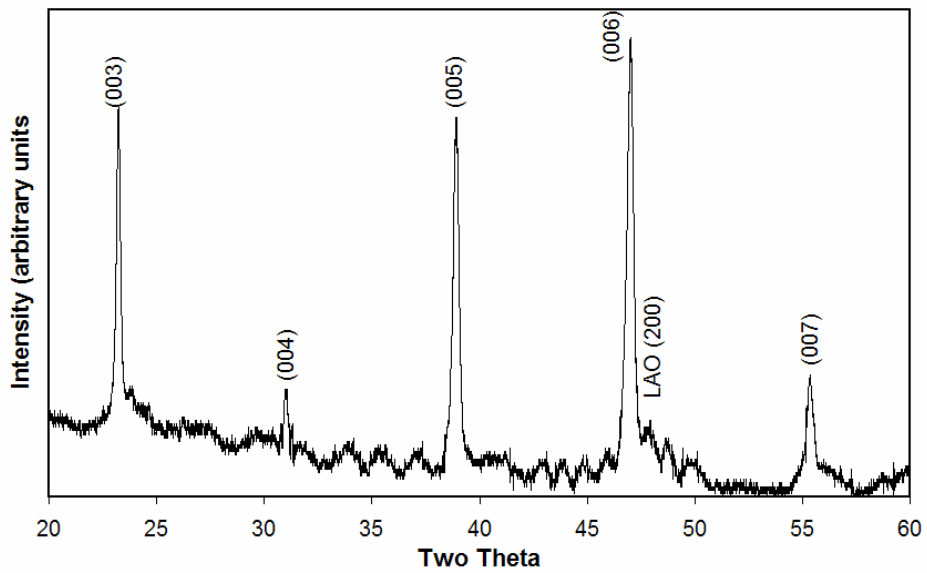

Figure 3.9: XRD pattern of YBCO film deposited by using TFA-MOD method. The film was heat treated at 800 °C.

3.2. YBCO Nanoparticle Method

3.2.1 Overview

As discussed earlier, the inherent problems in TFA-MOD process are the porosity, long process time and evolution of highly corrosive HF gas. An alternate approach starting with nanoparticles of Y-Ba-Cu-O as precursor was initiated by our group. A brief overview of the studies conducted in this thesis is given. Details of the results at every step is shown in the subsequent sections.

Initial experiments were carried out using Y-Ba-Cu-O nanoparticles in 1,4 butanediol ($C_4H_{10}O_2$) solvent without the use of any surfactant. A 4 % concentration of YBCO nanoparticle colloid was used in the experiments where we compared the chemistry and microstructure of the film processed using Nanoparticle method with that of the TFA-MOD processed film. From these results, it could be seen that to increase the processing speed and reduce porosity, therefore serve as an alternate approach to the TFA-MOD method. However the films fabricated still had porosity and inadequate superconducting properties.

Hence, higher concentration of particles was tried. It was realized that surface treatment of the substrate is essential in order to get a continuous film using these high concentration colloids. In these new films both porosity and processing time had significantly reduced. However, the critical temperature (T_c = 80 K) was low, critical current (I_c) was undetectable, and reproducibility was a concern. It appeared that the use

of a polymeric binder as an intermediate layer on the substrate might have detrimental effect on the film quality and epitaxy issues. Therefore, a new nanoparticle colloid with surfactant in the liquid was tried. The main idea behind the use of surfactant was to lower the surface tension and increase the wetting ability of the colloid. As expected, the use of any additional surface treatment of the substrate was eliminated with this new colloid. The films showed some improvement in T_c (82.5 K) and some I_c (0.57 A) was detected, but found to be very low. Different parameters like heating rate and concentration of copper was studied to improve the quality of the films, but no considerable increase in T_c and I_c was observed.

The beneficial results from these 1, 4 butanediol based experiments were (i) porosity was significantly reduced (ii) faster processing speed (iii) good texturing of YBCO films (iv) potential to fabricate thicker films using this route and (v) T_c and I_c were detected indicating superconductivity in these films. The problems that still existed were; low T_c and I_c in these films. It was suspected that the 1, 4 butanediol solvent which contain some impurities or the surfactant itself. It is also reported that viscosity of the solution in any liquid based technique has an effect on the film quality [57], so a new solvent which had lower viscosity was attempted.

Decanol has lower viscosity than the butanediol as it has only one OH group whereas butanediol has two OH groups and its boiling point is similar to butanediol (230 ^{o}C) which is requirement of the solvent used in this process. Films fabricated using this new decanol based colloid have shown very good results. The T_c has increased to 89

K which is comparable to that of our optimized TFA-MOD processed sample (88.5 K). Critical current density over 1 MA/cm^2 was detected in these films. The best result obtained till date with this method was 2 MA/cm^2, which took over a decade for the TFA – MOD process to achieve.

3.2.2 Comparison between TFA-MOD and Nanoparticle Processes

A 4% YBCO nanoparticle colloid was spin coated on MgO at the rate of 3600 rpm. The as deposited film was heat treated following the calcining heating profile of TFA- MOD process as shown in Fig 2.4. The chemistry of the sample was compared with that of the TFA-MOD processed sample.

Figure 3.10 shows the comparative XPS spectra of Y 3*d*, Ba 3*d*, and Cu 2*p* obtained from the samples after calcination using the Nanoparticle and the conventional TFA-MOD processes. In the Nanoparticle process, Y $3d_{5/2}$ peak observed at 156.7 eV can be attributed to Y_2O_3 according to the reported binding energy of 156.6 eV [49]. The Ba $3d_{5/2}$ peak is at 779.2 eV, which represents BaO according to its reported binding energy [51]. In case of TFA-MOD processed sample, the Ba $3d_{5/2}$ binding energy of 780.1 eV is attributed to BaF_2 and Y 3*d* binding energy of 157.6 eV is attributed to Y-O-F. The peak shapes of Cu 2p looks very similar in both cases. The Cu 2p binding energy analysis revealed that in both cases copper is bonded with oxygen. These films were fired to 800 ^oC following the heating profile given in Fig.2.5. XPS analysis on these samples showed

that the final chemistry is same for both Nanoparticle processed sample and TFA-MOD sample.

It is clear from XPS spectra analysis that in the Nanoparticle process, the calcined film has yttrium and barium ions bonded to oxygen, while in the TFA-MOD process, yttrium and barium ions in the calcined film are still bonded to fluorine, so additional chemical reaction will be required to expel fluorine containing gases, thereby resulting in higher porosity in the final film. The fluorine percentage which is one of the major disadvantages in case of TFA-MOD process is very minimal in the case of YBCO Nanoparticle processing. The raw atomic concentration of all the elements for the both films is given in table 3.1. The raw atomic concentration of fluorine in case of Nanoparticle process calcined film is only 2.6% when compared that due to TFA-MOD which is around 17.2 %. HF removal is not expected to be an issue in case of the Nanoparticle process due to very minimal amount of fluorine present. The final films had identical chemistry.

The next step was to check the surface morphology and texturing of the Nanoparticle processed film.

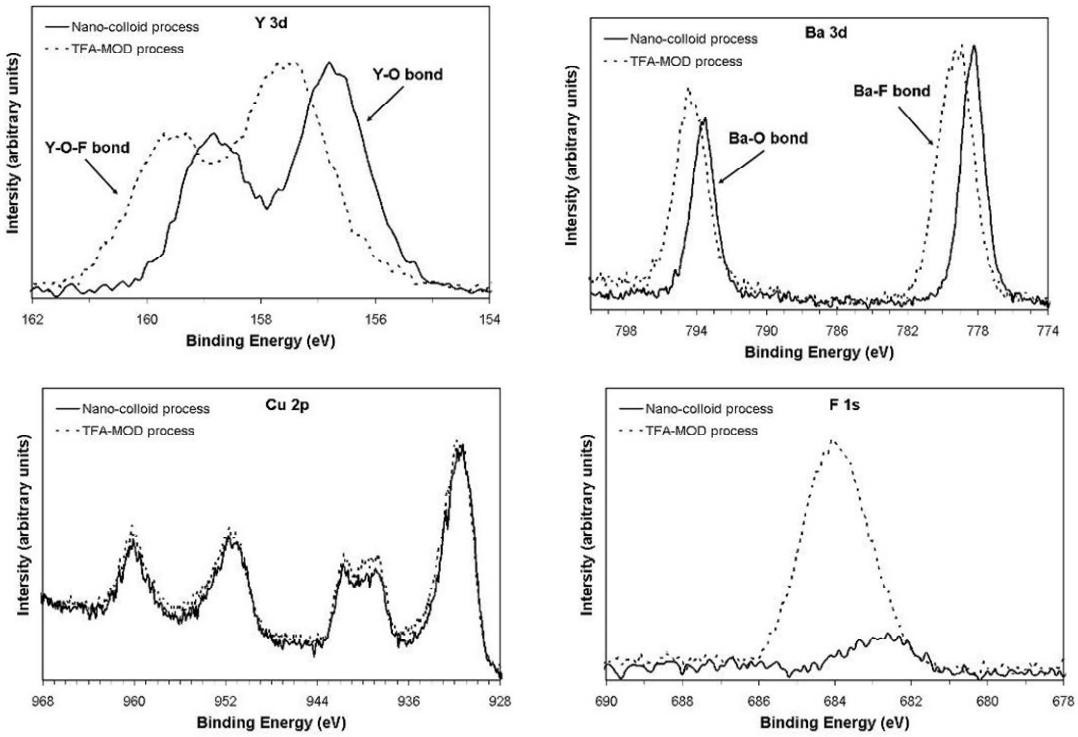

Figure 3.10: Comparison of High resolution XPS peaks in case of YBCO nanoparticle film heat treated till 400 ^{o}C and TFA-MOD calcined film till 400 ^{o}C.

Table 3.1: Quantified raw data taken on film prepared by YBCO nano solution and TFA processed precursor YBCO film (error = 3%)

% Atomic Concentration of	TFA processed precursor film(400 ^{o}C) (% ± 3)	Nanoparticle processed film (400 ^{o}C) (% ± 3)
Y 3d	3.9	2.3
Ba 3d	3.5	4.0
Cu 2p	25.5	26.7
O 1s	38.7	42.7
C 1s	11.4	19.7
F 1S	**17.0**	**2.6**

In order verify if the use of nanoparticle would result in higher processing speeds, as-prepared films using nanoparticle precursor and TFA-MOD precursor were calcined at fast rates (1 ^{o}C/min). Surface morphology of these films was studied using a SEM.

The TFA- MOD processed film has showed a lot of buckling as shown in figure 3.11. The Nanoparticle processed film was very smooth and uniform as shown in Fig. 3.12. Some adsorbed white particles were seen on the surface. EDS on these particles has indicated that they are Y-Ba-Cu-O compound. XRD observations showed that none of these films are crystalline yet. Higher temperatures were needed to crystallize the structure to form the superconducting phase.

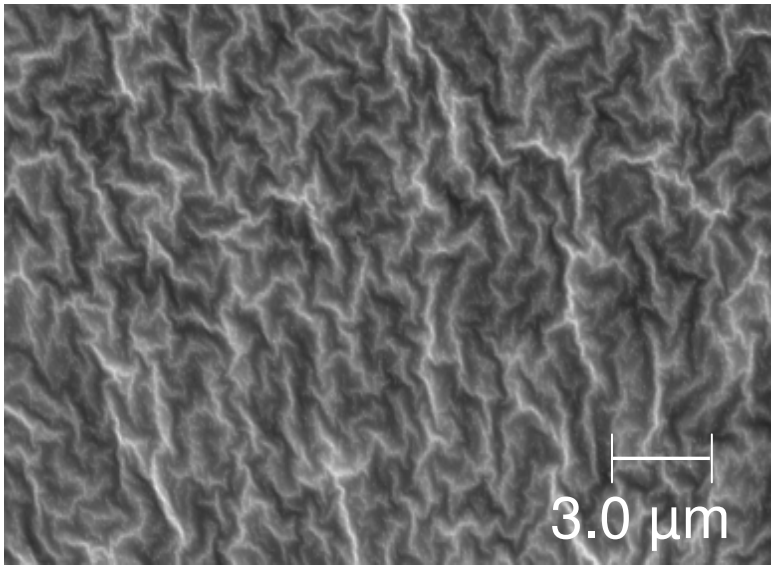

Figure 3.11: Microstructure of YBCO film prepared using TFA-MOD. The film was fired at 500 ^{o}C at the rate of 1 ^{o}C/min.

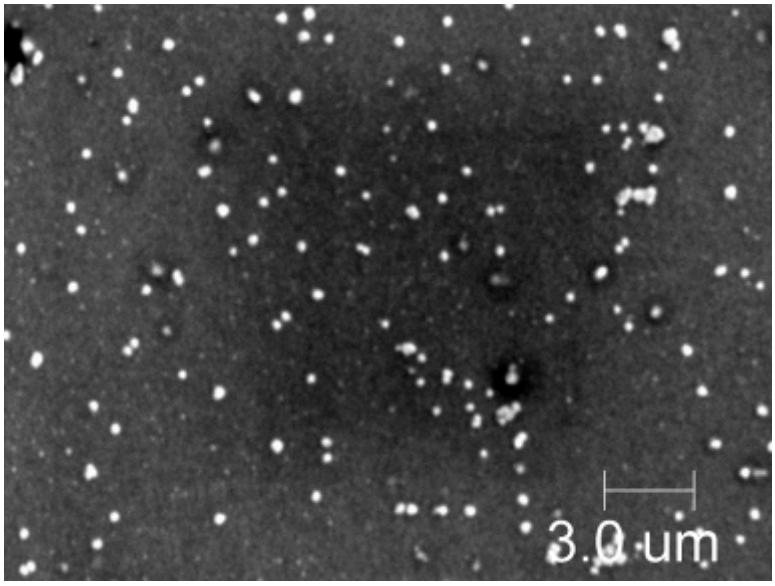

Figure 3.12: Microstructure of YBCO film prepared from solution dispersion of YBCO nanoparticles. The film was fired at 500 ^{o}C at the rate of 1 ^{o}C/min.

The 500^{o} C heat treated films were fired at 800 ^{o}C following the heating profile shown in fig 2.5 in order to check their surface morphology and texturing. The TFA-MOD film was crumpled and it had needle like growth with lot of defects as shown in Fig. 3.13. On the other hand, the Nanoparticle processed film showed c-axis oriented structure after 800^{o} C heat treatment as shown in Fig. 3.14. The XRD of this film has supported the fact that it is c-axis oriented YBCO crystal structure (Fig. 3.15). Some pores were also observed in this case, though lower than that of TFA films. It was determined that further optimization should be done to eliminate these pores.

From these initial results it was realized that the Nanoparticle method has a potential benefits and therefore may be used as an alternate approach to the TFA-MOD

method. But in order for that to really be the case, the superconducting properties need to be tested and processing needs to be optimized until comparable critical J_c and T_c are obtained. The following sections will discuss how this goal has been realized.

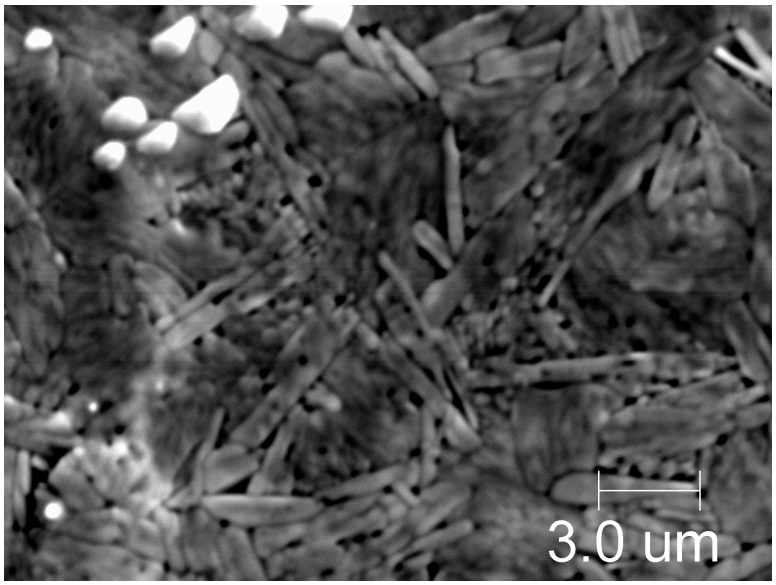

Figure 3.13: Microstructure of YBCO film prepared using TFA-MOD process. The film was fired at 800 ^{o}C.

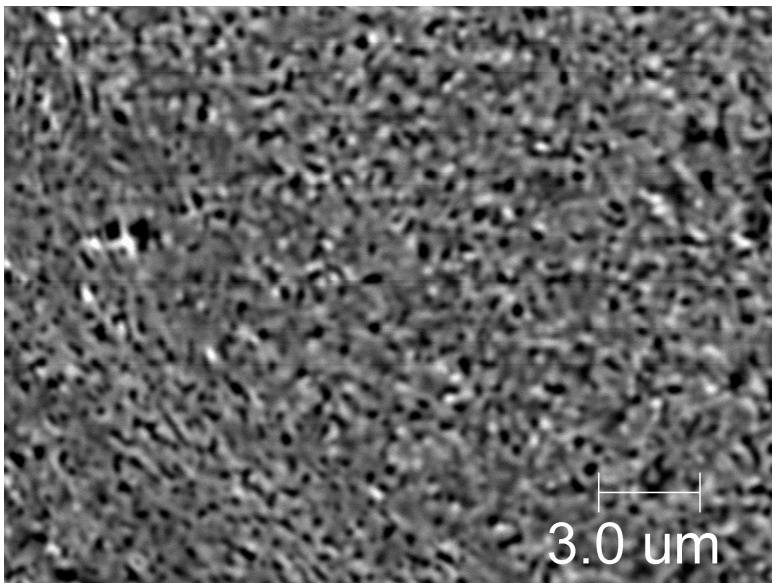

Figure 3.14: Microstructure of YBCO film fabricated by using 4% nanoparticle solution. The film was heat treated at 800 °C.

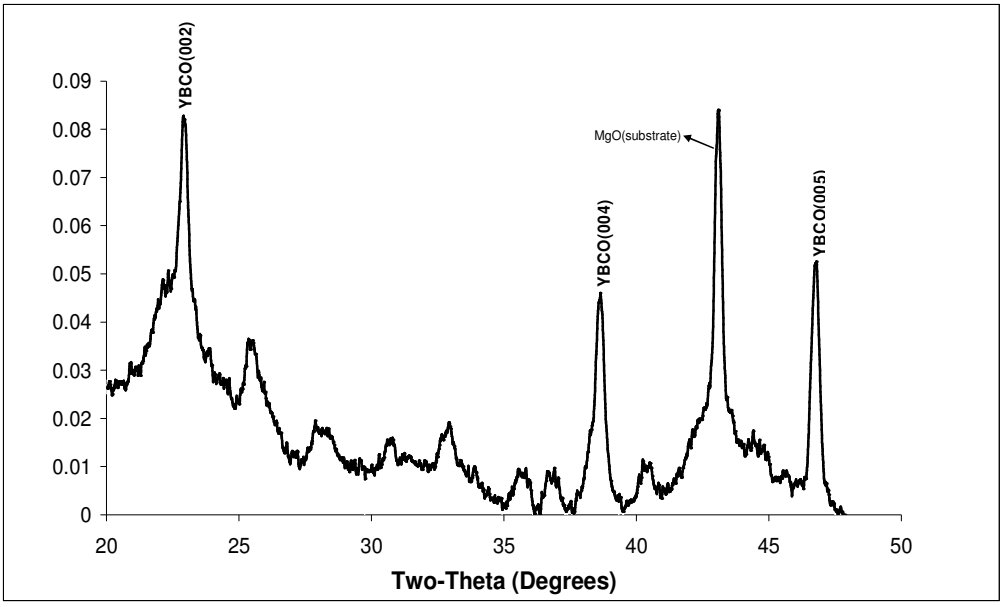

Figure 3.15: XRD pattern of YBCO film deposited by using nanoparticle method. The film was heat treated at 800 °C.

3.2.2 Concentration of Nanoparticulate Dispersion

The films fabricated using a 4% YBCO nanoparticle colloid were porous and discontinuous. One of the approaches that can be used to reduce pores in the film was to increase the solid loading of the nanoparticles in the suspension. Three different concentrations (6%, 15%, 20%) of nanoparticles in the colloid were tried for fabricating the films.

6 % YBCO Nanoparticle Colloid:

The main problem with the colloids of higher nanoparticulate concentration was the wetting of the colloid with the LAO substrate. A polymeric binder was used as an intermediate layer before applying the nanoparticle coating (the chemistry of the binder used is not disclosed due to proprietary concerns). Once this problem was solved, the other problem faced was degree of shrinkage of film, when it was heated to 250 ^{o}C at the rate of 1 ^{o}C/min. Different heating rates were tried. A faster heating rate like 10 ^{o}C/min worked out better. The reason for this behavior might be due to the slow evaporation of the solvent, which was holding the particles apart, and would give enough time for the particles to agglomerate. So during the faster heating rate, the time was not enough for the particles to aggregate and form as a lump. The optimized heating rate was found to be 3 ^{o}C/min.

The calcined sample was fired to 800 ^{o}C following the heating profile given in Fig 2.5. The surface microstructure of this fired film is shown in Fig. 3.16. The films looks very dense with c-axis oriented grained. White particles were observed on the film, EDS reveals that these are copper rich zones. The sample showed room temperature resistance of 100 ohms. The T_c detected on this sample was 80 K with transition width of 2.3 K (Fig. 3.17), which is very low when compared to the optimized TFA-MOD processed film (88.5 K). The low T_c values and the observed broad transition can probably be attributed to the formation of other second phases and the low oxygen content in the YBCO structure. The I_c of the films is undetectably small and this was likely due to the low T_c and the presence of secondary phases. Concentration was further increased to see the effect on film morphology and electrical properties.

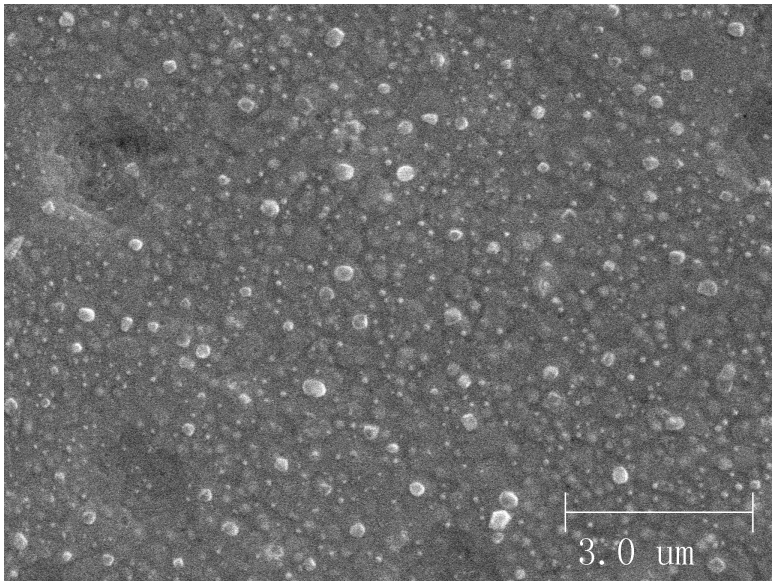

Figure 3.16**:** Microstructure of YBCO film fabricated using 6% YBCO nanoparticles solution. The substrate was treated with RCA protocol solution and intermediate polymeric binder layer as applied before the nanoparticle coating.

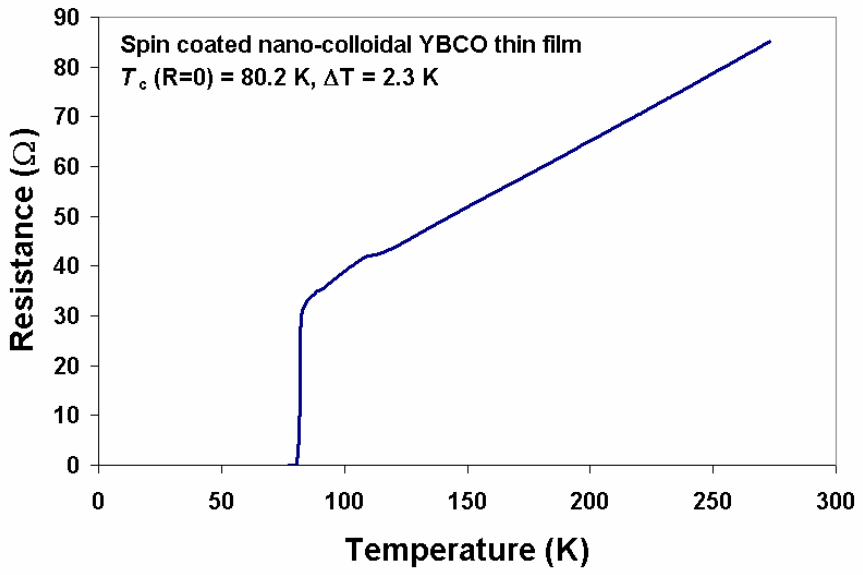

Figure 3.17: T_c data for film fabricated using 6% YBCO nanoparticles solution after the surface treatment of LAO substrate with polymeric binder layer.

15% and 20% YBCO nanoparticle colloid:

The concentration of nanoparticle was increased further to 15% and 20% to study the effect of higher concentration on surface morphology of films. The problem with these higher concentrations was that the nanoparticles started to precipitate out of the coating after a short period of time, making the film chemistry inhomogeneous. When a thick layer of polymeric binder is used as a pre-coating the problem of precipitation is solved. The thick layer of polymeric binder is formed by placing the polymeric binder coated substrate on a hot plate preheated to 100^{o}C immediately after coating. The polymeric binder evaporated right away like a steam forming a thick layer of coating on the substrate. The pre-coated substrates were dip coated or spin coated with 15% and 20% nanoparticle colloid. The room temperature resistance in case of 20% and 15% nanoparticles coated final YBCO films were 56 ohms and 16 ohms respectively. The

transition temperature for R=0 was 81 K in case of 15% where as 80 K in case of 20%. The I_c of the films was undetectably small. The 20% coated film showed a lot of a-axis orientation (Fig. 3.18). XRD result also showed a strong presence of a-axis oriented grains (Fig. 3.19). The presence of a-axis grains causes deterioration of critical current I_c of a superconductor.

These results indicated that use of higher concentrated colloid for fabrication of films would not have any positive effect **without additional surface treatment of the substrate.** Surface treatment may enable formation of uniform coatings. The concentration of nanoparticles did not have considerable effect on the T_c. The measurable critical current was still not achieved which might be due to the secondary phases and defects. Reproducibility has become an issue in this procedure. The use of polymeric binder as an intermediate layer may be one of the reason. So a colloid with surfactant is tried.

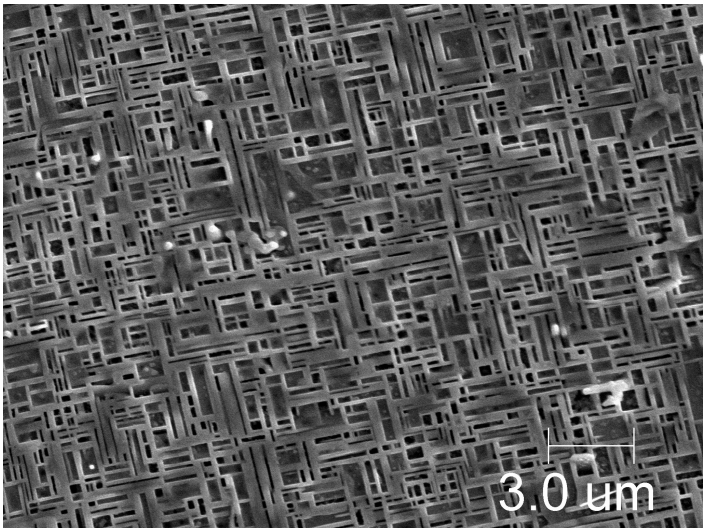

Figure 3.18: Microstructure of final film prepared using 20% YBCO nanoparticle concentration on LAO substrate with polymeric binder layer.

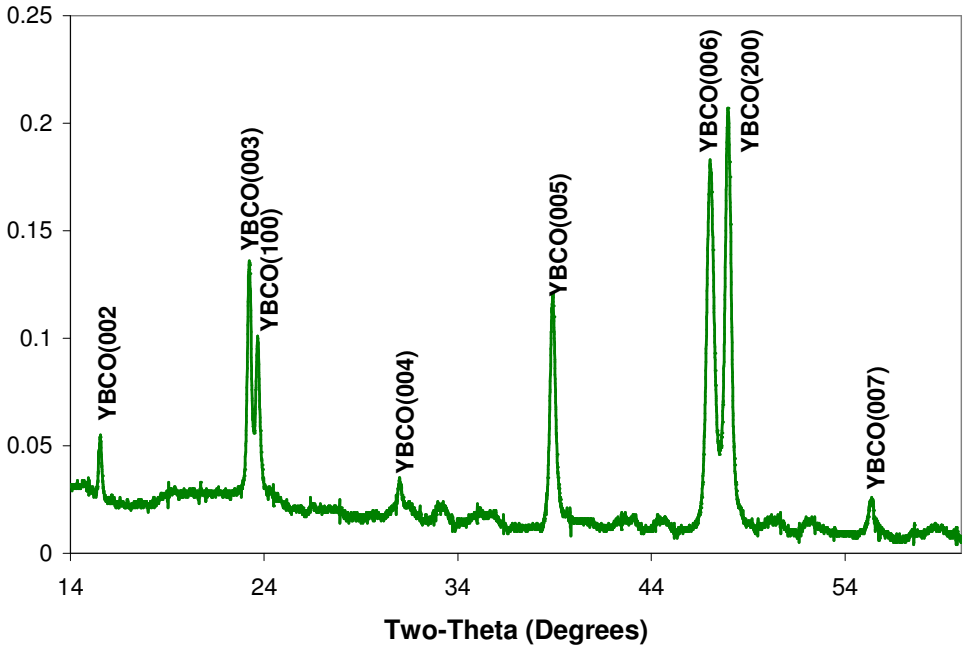

Figure 3.19: XRD of final film prepared using 20% YBCO nanoparticle concentration on LAO substrate with polymeric binder layer.

3.2.3 Effect of Surfactant in the Colloid on the Film

Surfactant is used to decrease the surface tension of a liquid and increase the wetting ability of the colloid with the substrate. A nanoparticle colloid with a surfactant was used to check if surfactant improvements were possible. 13% nanoparticle colloid was used in this study. The use of a surfactant inside the colloid has solved the problem of wetting the substrate which was encountered in previous experiments.

Nanoparticle precursor coating was applied on the substrate either by dip coating or spin coating. These as prepared films were calcined to 400^{o} C following the temperature profile which has been optimized as given in Fig. 2.6. The precursor film was then fired to 800 ^{o}C following the heating profile given in Fig. 2.5. Figure 3.20 show an SEM image of the surface of the final film. The coating looked uniform and dense with some a-axis orientation. White particles seen in the microstructure were found to be copper rich zones using EDS. The room temperature resistance of this sample was found to be 5 ohms. The critical temperature of this sample was found to increase to increase to 82.5 K (Fig 3.21). I_c was detected for the first time in these samples. It was measured to be only 0.57 A (Fig. 3.22). One of the reasons for low the I_c can be the presence of white copper rich zones which lower the critical current.

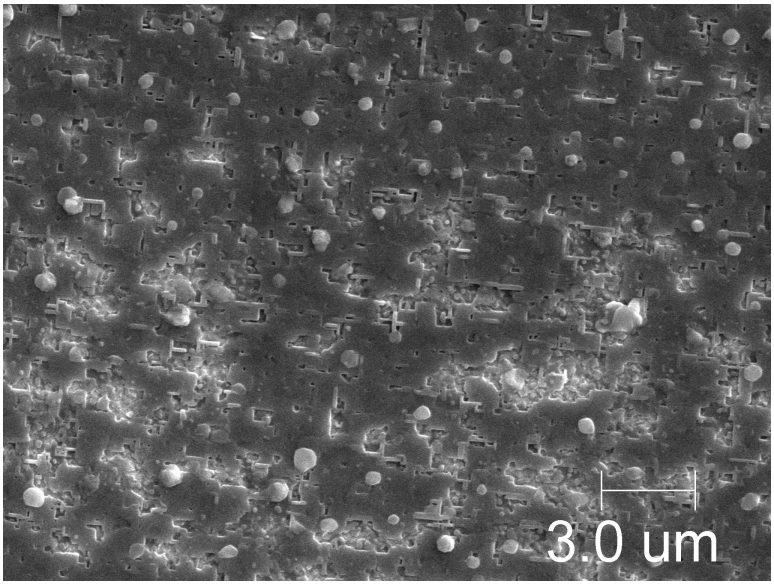

Figure 3.20: Surface Morphology of the film fabricated using 13% YBCO nanoparticle colloid with surfactant on LAO substrate.

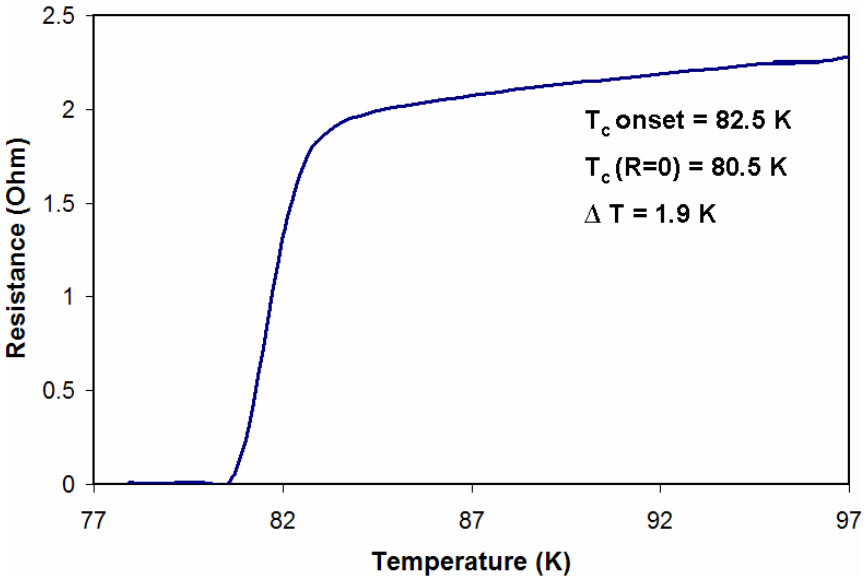

Figure 3.21: T_c data for film fabricated using 13% YBCO nanoparticles solution with surfactant on LAO substrate.

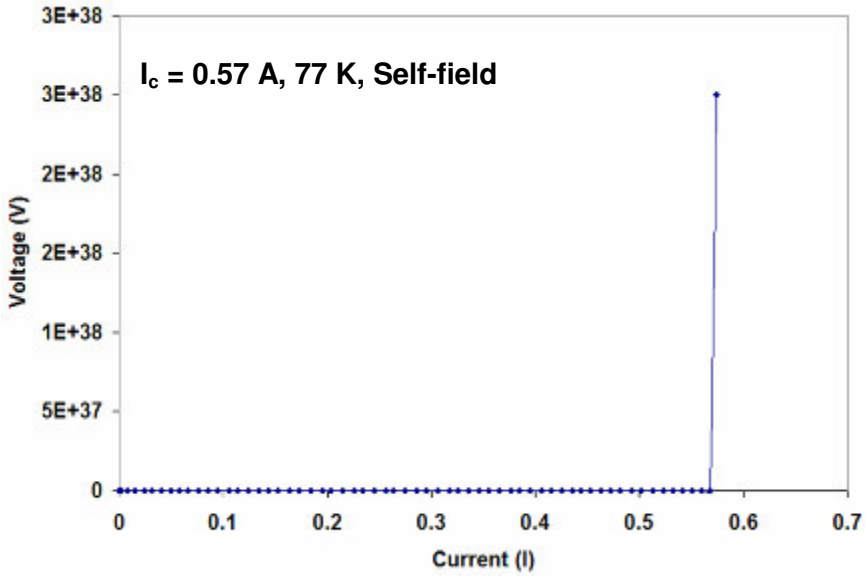

Figure 3.22: I_c data for film fabricated using 13% YBCO nanoparticles solution with surfactant on LAO substrate.

These results have shown that surfactant in the colloid has positive effect on the processing of film. As expected, there was no necessity of substrate surface treatment as the surfactant has affected the wetting ability of the colloid with the substrate, as was expected. The total time for the calcination of film was less than 6 hrs as compared to the 19 hrs for TFA-MOD. Dense, continuous and textured films have been fabricated with this colloid, porosity was considerably reduced, critical current was detected and there was minor improvement in critical temperature. The reason for poor T_c and I_c might be due to the presence of any impurities or formation of secondary phases in the final films. XPS was used to check for any impurities or secondary phases present in the films.

XPS analysis was done on the sample fabricated using a colloid with surfactant. As mentioned earlier, PLD samples have best stoichiometry since it is a direct transfer from the YBCO target onto the substrate. Therefore, XPS spectra of the final films fabricated using the Nanoparticle method were compared with that of the YBCO film fabricated using PLD process. XPS analysis shows that the whole chemistry of the as prepared film is similar to that of the PLD processed YBCO (Fig. 3.23). It was observed that the film contained only Y, Ba, Cu and O elements. Raw quantification data of both films is shown in table 3.2. From raw quantification data it is observed that Cu atomic % was low in the nanoparticle films when compared to that of PLD films.

From these XPS results it was found that the film did not contain any impurities and the chemistry of the film is similar to that of a PLD film. The possibility of impurities can not be totally neglected since XPS has limitations detecting elements with concentrations

below 2%. It was also noticed that copper atomic percentage was low in case of Nanoparticle processed sample when compared to that of PLD sample. It has been observed by Santiso et al. [56] that the critical temperature decreases with the decrease in copper content in the film. The effect of concentration of copper on the film properties will discussed in the next section.

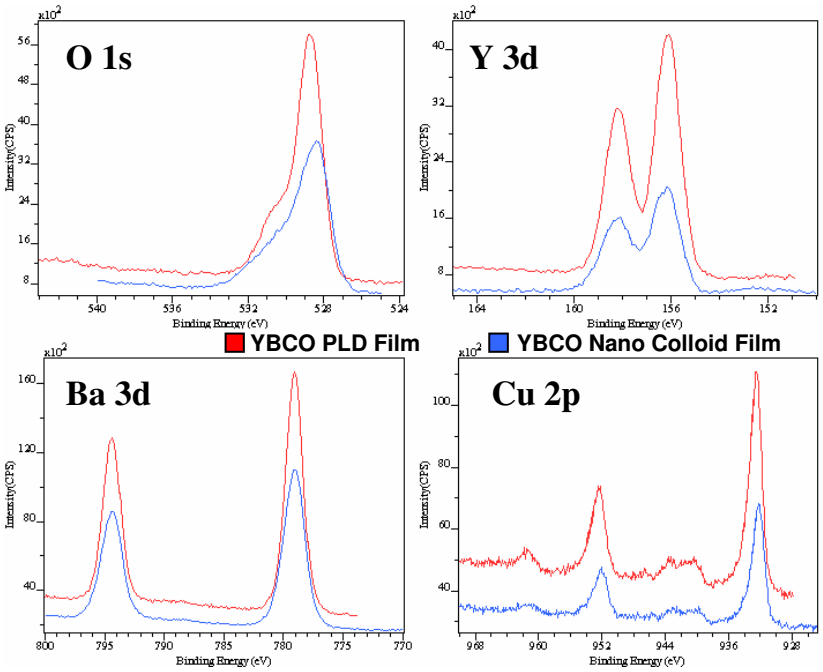

Figure 3.23: XPS peaks comparison between YBCO final film formed by 13 % YBCO nanoparticles colloid and YBCO film fabricated by PLD process

Table 3.2: Quantified raw data taken on films prepared by 13% YBCO nano colloid and PLD processed YBCO

% Atomic Concentration of	PLD processed YBCO	13% YBCO Nanoparticle processed film (800^{o}C)
Y 3d	11.3	8.3
Ba 3d	15.1	16.5
Cu 2p	24.9	20.2
O 1s	48.7	55.0

3.2.5 Effect of concentration of Copper on YBCO thin films

One of the factors that might affect the critical temperature (T_c) is the concentration of copper in the colloid [56]. There is a possibility of copper loss during the calcining and firing treatment, leaving the film deficient in copper. Experiments were performed to see the effect of excess copper percentage on the film properties. Films are fabricated with 5%, 10%, and 15 % excess copper in the colloid.

Figures 3.24 – 3.26 shows the SEM images of the surface morphology of the YBCO films, indicating a similar microstructure observed for all the samples. Films had copper- rich zones and fine (Cu, Ba) rich zones. The critical temperature measurements are shown in Fig. 3.27. There was no considerable change in the critical transition temperature, which is about 80 K (R=0) in all three cases. Note that a higher second transition was observed in all curves, as show in inset of Fig. 3.27, indicating the formation of secondary phases in these films. Figure 3.28 shows critical currents measured in samples with variation of concentration Cu. The highest critical current was observed on the film with 10% copper excess. All the samples fabricated had similar dimensions.

These results show that the variation of Cu content does not have a significant effect on the microstructure and transition temperature. Though there is a change in the I_c values, this could either due to the copper effect, or the sample microstructure, or the defects present in the sample.

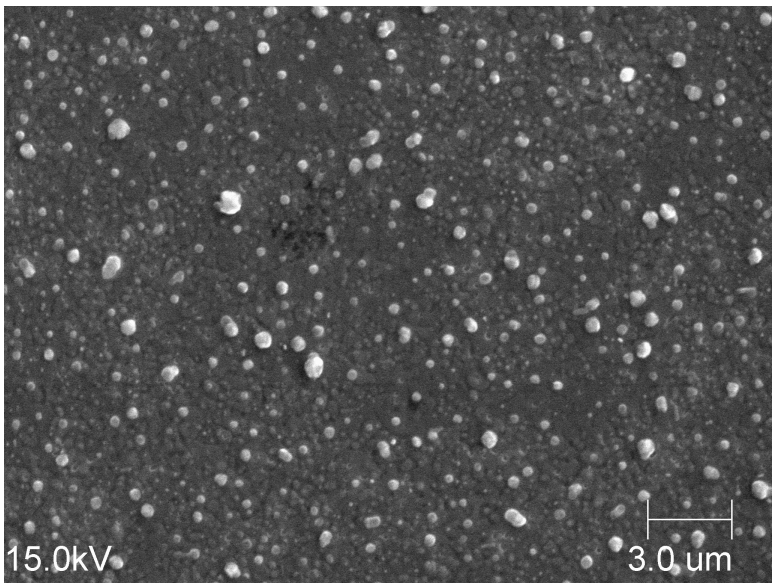

Figure 3.24: Surface morphology of film fabricated using 5% excess copper concentration in the colloid

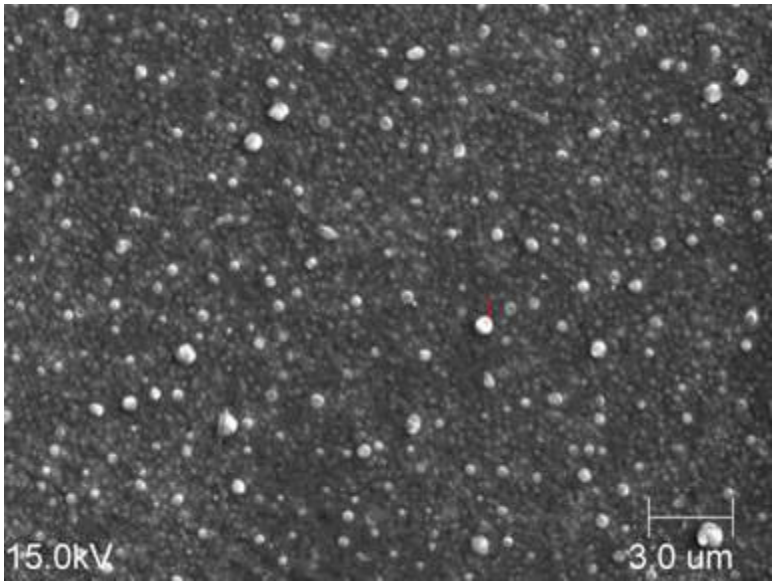

Figure 3.25: Surface morphology of film fabricated using 10% excess copper concentration in the colloid

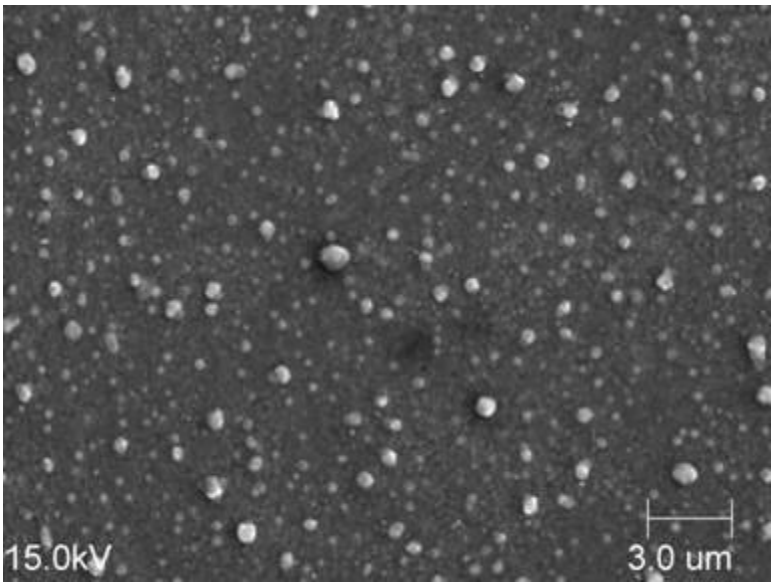

Figure 3.26: Surface morphology of film fabricated using 15% excess copper concentration in the colloid

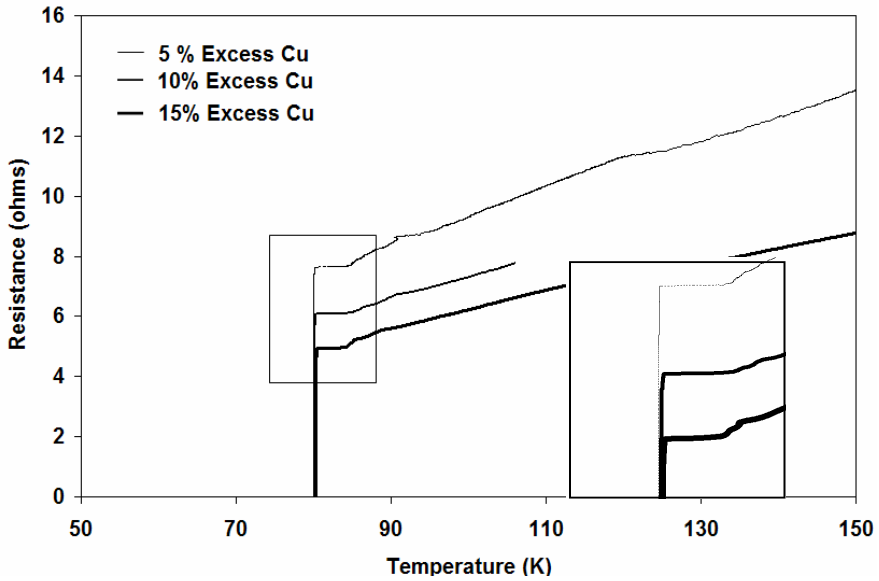

Figure 3.27: Effect of concentration of copper in the solution on the T_c of the YBCO films

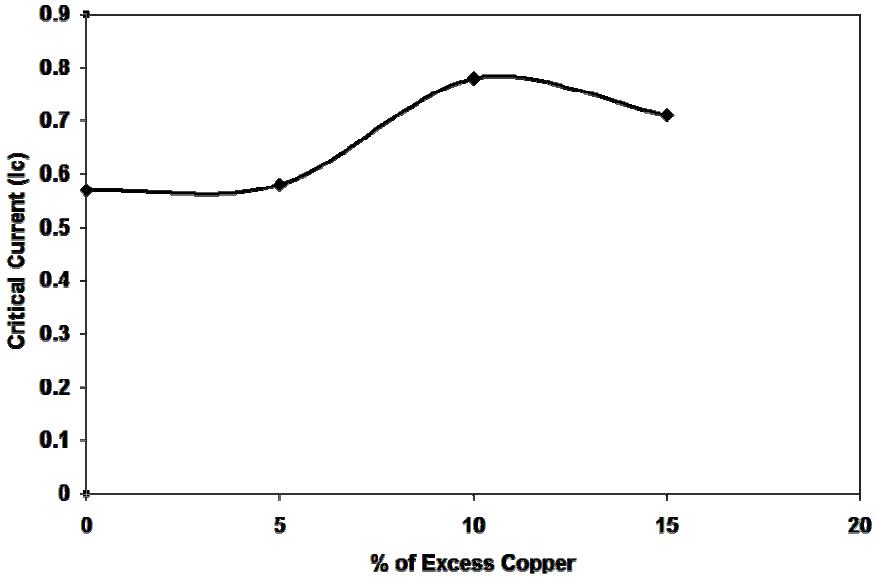

Figure 3.28: Effect of concentration of copper in the solution on the Critical Current of the YBCO films

3.2.8 Fabrication of Thick YBCO films using Nanoparticle Process:

There are several different ways to control YBCO film thickness in the Nanoparticle method: by varying the concentration of nanoparticles in the coating colloid, changing acceleration time and/or spinning rate, and making multiple coatings. However, by controlling acceleration time or spinning rate, striation in the gel film is observed for spinning rate of over 5000. Then spinning rate was fixed at 3600 rpm and film thickness was controlled by varying the concentration of nanoparticles of the coating colloids.

Films were fabricated using 13% and 18% nanoparticle concentration by spin coating the colloid onto LAO single crystal at a rate of 3600rpm for 3 minutes. The cross sectional SEM pictures of these films are shown in Fig. 3.29 and Fig. 3.30. The average

coating thickness of the sample fabricated using 13% nanoparticle concentration colloid is 0.35 µm where as that for 18 % nanoparticle concentration colloid is 0.63 µ. It is clear that the thickness of the film increases with the concentration of the nanoparticles. The T_c of the films had no change.

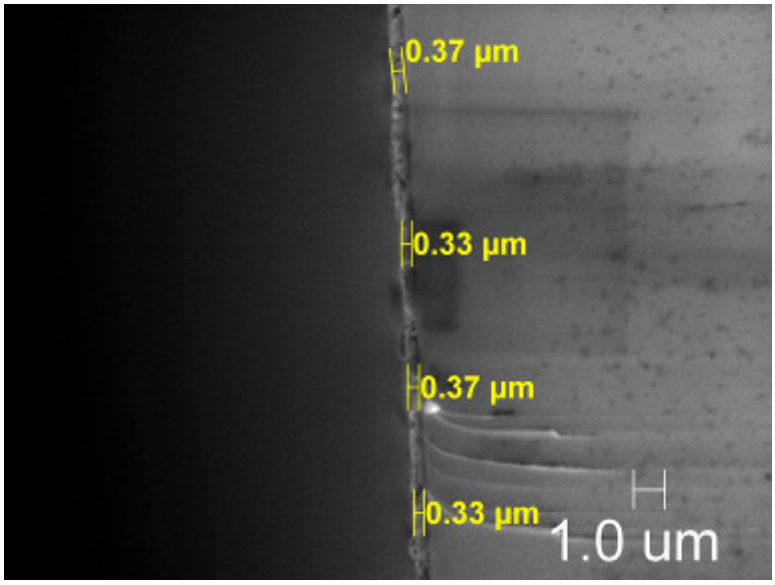

Figure 3.29: Cross-sectional view of film fabricated using 13% nano particle solution

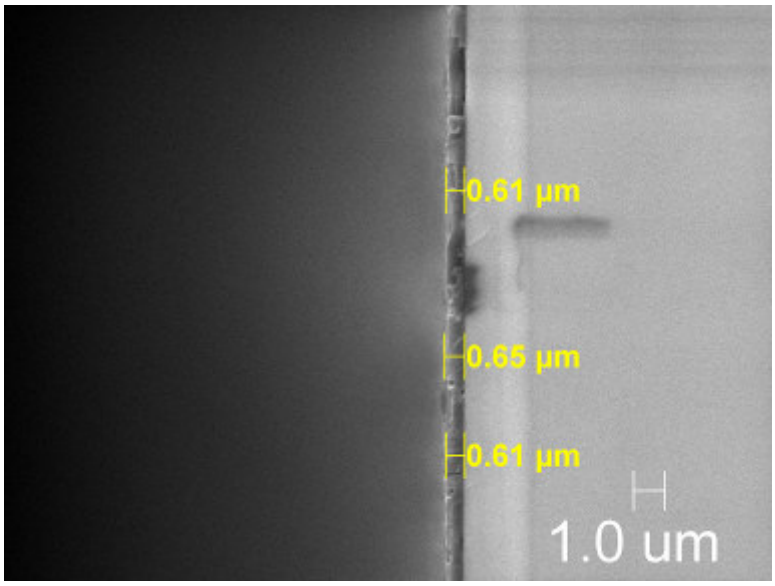

Figure 3.30: Cross-sectional view of film fabricated using 18% nano particle solution

In summary, the butanediol based colloids with surfactant inside has successfully fabricated dense and continuous YBCO thin films. The porosity has been significantly reduced in these films when compared to that of TFA-MOD processed films. The total processing time for the fabrication of the precursor film has greatly reduced (~ 6 hrs) when compared to that of TFA-MOD process (~ 19 hrs). Good texturing was observed in these films. There is a potential to fabricate thicker films with this method. In spite of these good outcomes the problem of low T_c and I_c still exits. The reason might be due to the 1, 4 butanediol solvent which might contain some impurities or the surfactant itself. It was also reported that viscosity of the solution has an effect on the film quality [57]. For all of these reasons, new solvent was used to fabricate the films.

3.2.6 Fabrication of YBCO Thin Film using Decanol Solvent

The films fabricated using butanediol based colloid did not show substantial improvement in the critical current and critical temperature. The manner in which the butanediol solvent behaves with the nanoparticles might have an effect on the film properties. It was also reported that viscosity of a solution plays a very important role on the final film quality [57]. So a solvent with lower viscosity would be favorable for fabricating these thin films. Decanol (CH_3 $(CH_2)_9OH$) has only one -OH group compared to that of butanediol which has 2 -OH groups, so the viscosity of decanol is lower than that of butanediol. Moreover, the boiling point of decanol is similar to that of butanediol (230 ^oC) making it a good solvent for these experiments.

Samples are prepared using dip coating and spin coating with decanol based 12% nanoparticle colloid with out surfactant and following the heating profile similar to that used for butanediol based nanocolloid. The colloid had very good wetting ability with substrate. The surface microstructure of the film is shown in Figure 3.31. The film is sightly more porous when compared to that fabricated using a butanediol based solvent.. However the porosity is significantly low that that of TFA films. The film has very low concentration of a/b-axis grains. XRD data also supports the same (Fig. 3.32). The critical temperature (T_c) at R=0 of the film increased to 89 K (Fig. 3.33) which is comparable to that of the optimized TFA-MOD processed sample (88.5). From the raw quantification data (table 3.3) obtained from XPS it is observed that the stoichiometry of the film is very close to the PLD YBCO.

The critical current density of the film measured using the four point method was 2 MA/ cm^2 (Fig. 3.34), which is a big achievement in this work as it has taken more than a decade for the TFA-MOD processed sample to get to this value.

The porosity in the film is not desirable since it affects the durability of the film. The problem may be solved by fabricating the film with a higher loading of nanoparticles. Films were prepared using 16 % YBCO nanoparticles colloid following the same heat treatment. Figure 3.35 shows the SEM picture of microstructure of this film. The porosity is considerably reduced while retaining the same transport properties. From this result it is believed that using decanol as a solvent has a positive effect on the superconducting properties of the YBCO film.

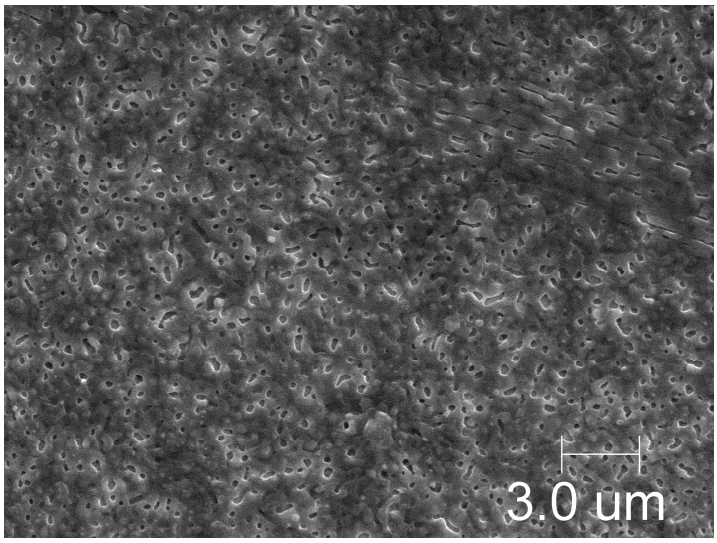

Figure 3.31: Surface morphology of film fabricated using 12% YBCO nanoparticles in a Decanol Solvent

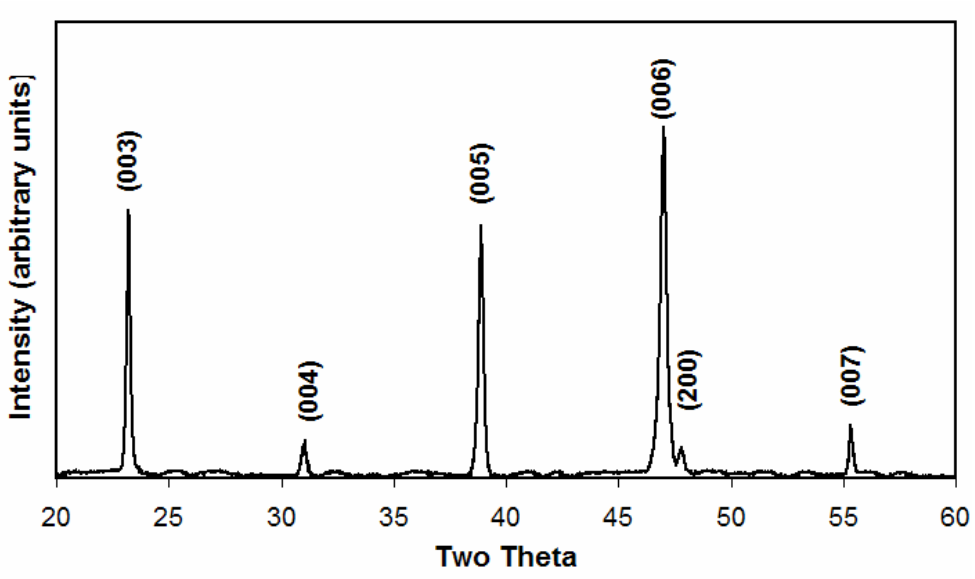

Figure 3.32: XRD taken on film fabricated using 12% YBCO nanoparticles in a decanol solvent on LAO substrate.

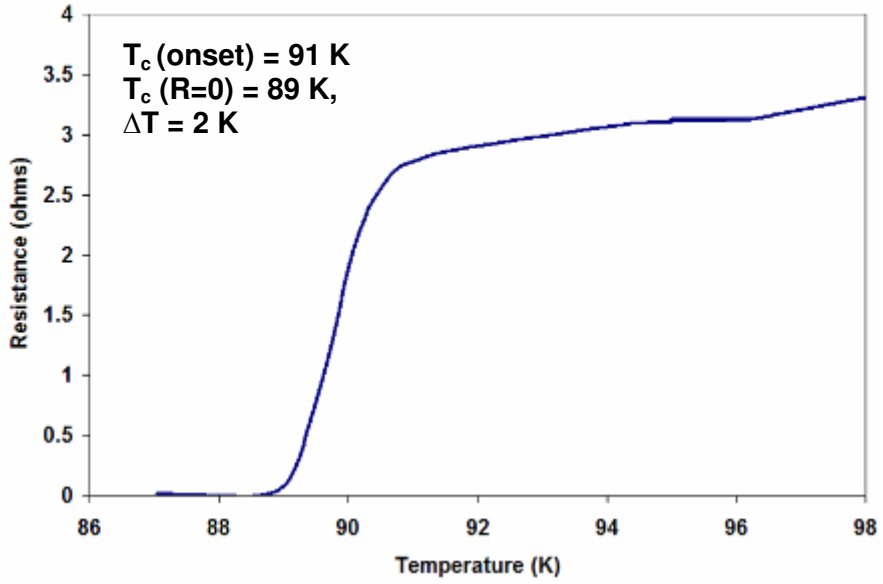

Figure 3.33: T_c data for film fabricated using 12% YBCO nanoparticles in a decanol solvent on LAO substrate.

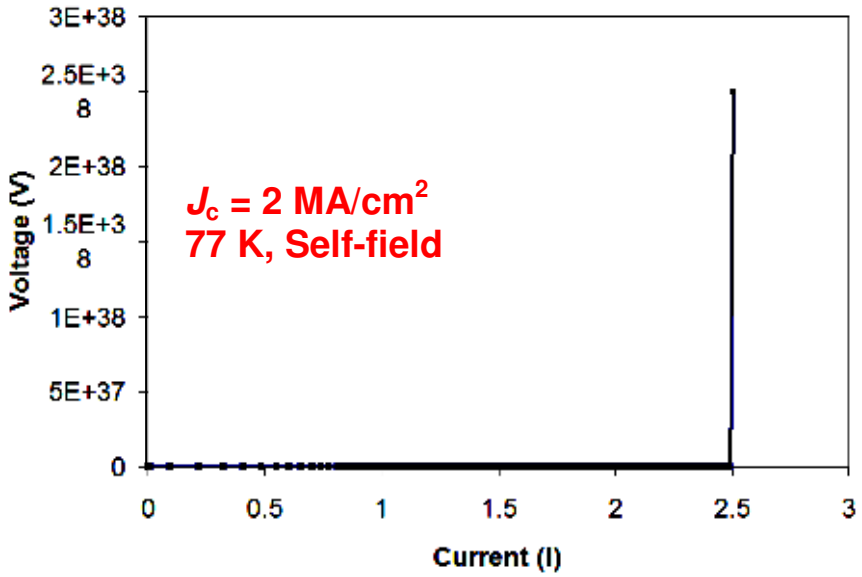

Figure 3.34: I_c measurement on film fabricated using 12% YBCO nanoparticles in a decanol solvent on LAO substrate. Film size: 10mm long, 100nm thick with 0.88mm bridged width

Table 3.3: Quantified raw data taken on film prepared by 12% YBCO nanoparticles in a decanol solvent on LAO substrate (error percentage - 3 %).

Atomic %	Oxygen	Yttrium	Barium	Copper
Film made with decanol based colloid	52.5	8.3	17. 0	22.2
Film Processed using PLD method	48.7	11.3	15.1	24.9

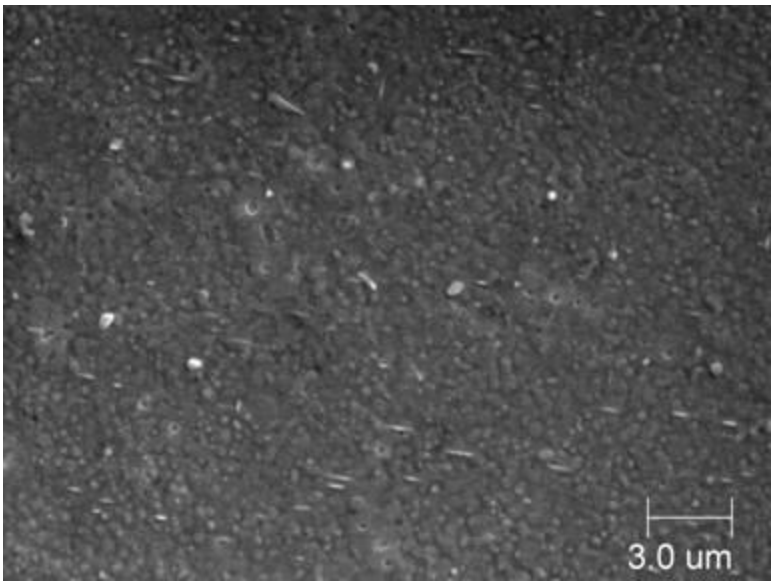

Figure 3.35: Surface morphology of film fabricated using 16% YBCO nanoparticles in a Decanol Solvent. This indicates that a dense YBCO film can be processed rapidly using the nanoparticle approach. This film had J_c = 2.0 MA/cm^2 and T_c = 89 K and indicates a new method of forming superconducting oxide using a new liquid phase process

3.2.7 Effect of Firing Temperature on Microstructure of YBCO Film

The effect of firing temperature on the film properties was studied by firing the films at 700^o C, 750^o C, 800^o C, 850^o C and 900^o C. Figures 3.36 – 3.40 show the high magnification SEM images of the surface morphology of the respective YBCO films, indicating that the film microstructure changes with the firing temperatures. As the firing temperature increases, the microstructure became denser and the grains grew further. At the temperatures of 700^o C and 750^o C the surface had lot of a- axis oriented grains and a

very porous structure (Fig. 3.36 and Fig 3.37). As the firing temperature increased to 800^{o} C and 850^{o} C the number of a-axis grains is greatly reduced (Fig. 3.38 and Fig. 3.39) and they disappeared totally at 900 ^{o}C (Fig. 3.40). At 900^{o} C the surface became irregular and secondary phases formed on the surface. EDX on these particles has shown that they are Ba and Cu rich phases. Hence it is believed that at 900 ^{o}C YBCO is partially decomposed. The variation of grain orientation with firing temperature can be explained by lattice mismatch. The variation of I_c for the films with firing temperature is shown in Fig. 3.41. The films fabricated have similar dimensions. The I_c has considerably increased from 700 to 850 ^{o}C and decreased slightly as the firing temperature increased. The I_c is not detectable in the case of samples fired at 700 ^{o}C and 750 ^{o}C, which might be due to the a- axis oriented grains. The degradation of I_c at 900 ^{o}C seems to be related to the secondary phases. The highest I_c was observed for samples fired at 850 ^{o}C which can be attributed to factors such as enhanced phase purity, texture, moderate film density and grain size.

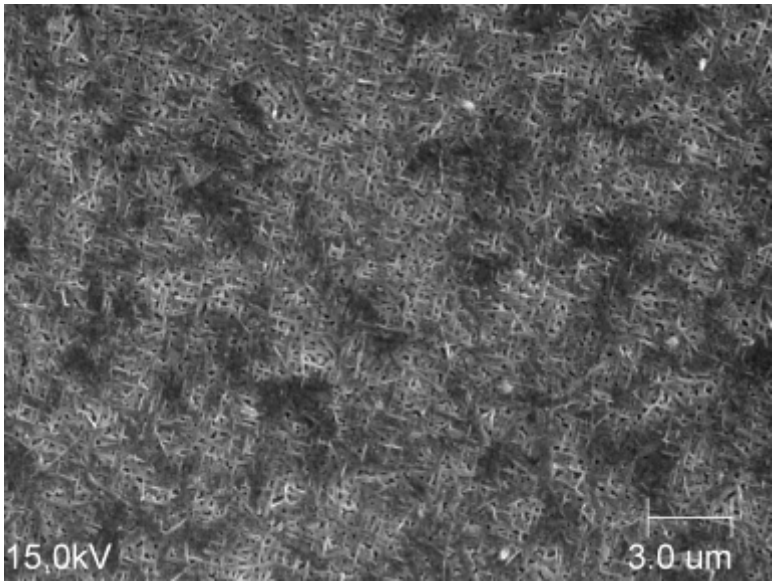

Figure 3.36: Surface morphology of YBCO film fired at 700^{o} C for 1 hr after calcining at 400^{o} C

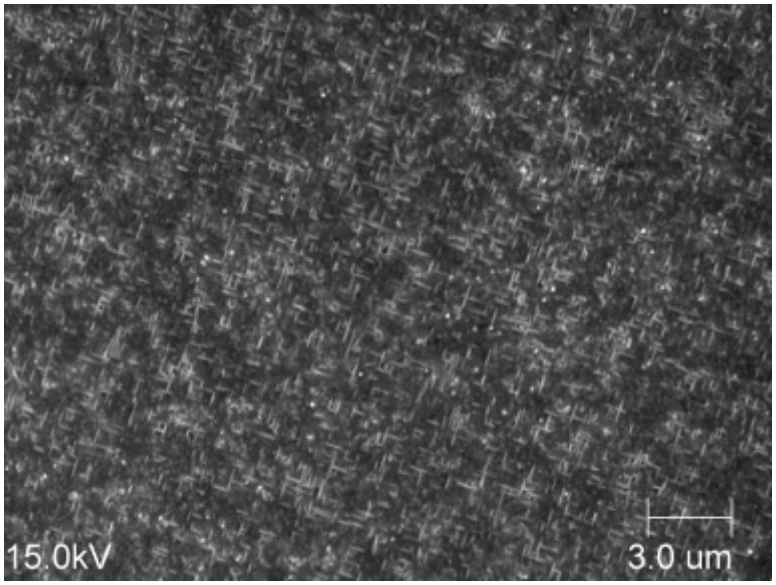

Figure 3.37: Surface morphology of YBCO film fired at 750^{o} C for 1 hr after calcining at 400^{o} C

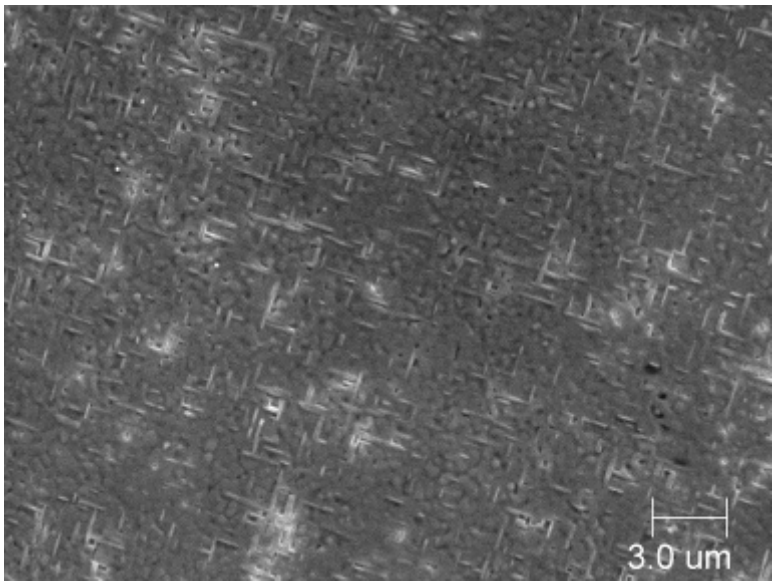

Figure 3.38: Surface morphology of YBCO film fired at 800^{o} C for 1 hr after calcining at 400^{o} C

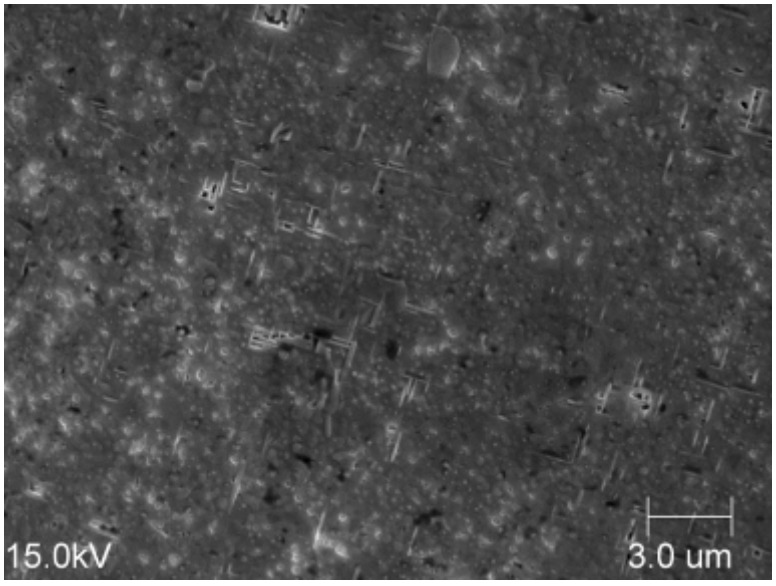

Figure 3.39: Surface morphology of YBCO film fired at 850^{o} C for 1 hr after calcining at 400^{o} C

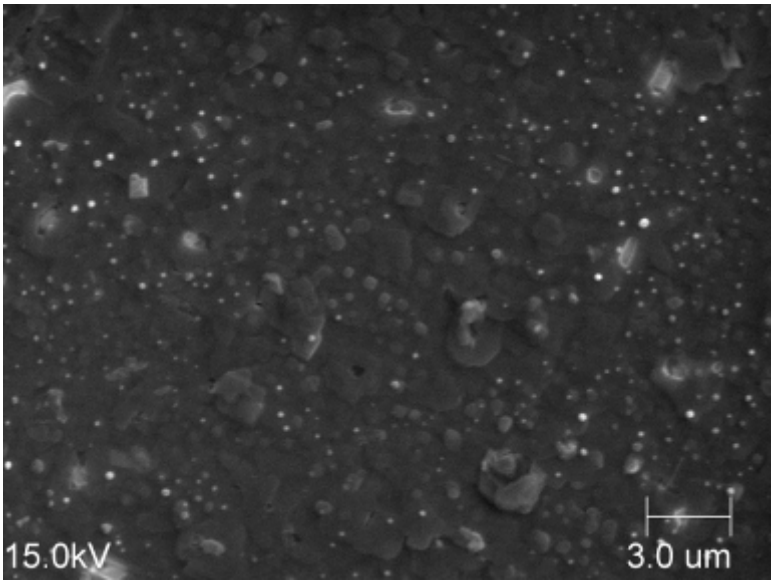

Figure 3.40: Surface morphology of YBCO film fired at 900^{o} C for 1 hr after calcining at 400^{o} C

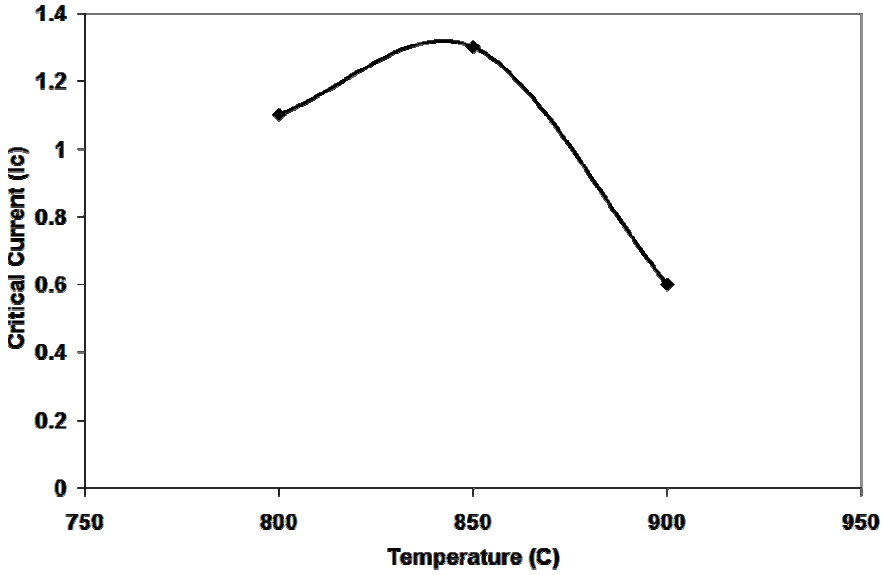

Figure 3.41: Effect of Firing Temperature on the Critical Current of the YBCO films

In summary, the use of decanol as a solvent had produced very promising results. The colloid had very good wetting ability with the substrate. Hence the use of surfactant is totally eliminated in the decanol based process, in turn giving us a better control on the process. The films were fired using the same profile as that used for butanediol based samples. The films had very good texturing; porosity has been significantly reduced when high concentrated colloids were used. The films are dense and continuous. The critical temperature (T_c = 89 K) of the superconducting thin film obtained using this decanol based colloid is comparable to that of our optimized TFA – MOD (T_c = 88.5 K). Critical current densities over 1 MA/cm^2 are routinely obtained using this method. The best result so far is 2 MA/cm^2, which has taken over a decade to achieve for TFA-MOD processed sample. Further optimization of the process is needed in order to get better results. However, the current results are very promising for the use of the Nanoparticle method in fabrication of second generation superconductors.

4. SUMMARY & FUTURE WORK

4.1 Summary

Detailed investigations on the chemical reactions that occur during the fabrication of YBCO using the TFA-MOD process have been performed using XPS. It has been observed that all the acetates and fluorocarbon groups are removed after calcination process. The calcined film mainly consists of Y, Ba, Cu, O, and F, where Yttrium is present as Y-O-F, Barium as BaF_2, and Copper is in form of CuO. During the early stages of firing, Barium is still in fluoride form but after firing all the fluorine is eliminated as HF gas leaving Barium in oxide form in the final film.

The influence of heating rate during the calcining process in TFA-MOD process on film chemistry, microstructure, and electrical properties has been investigated. The heating rate does not change the overall chemistry of calcined films but the surface morphology of the calcined films depends on heating rate. The 3 ^{o}C/hr calcined film resulted in a uniform, smooth calcined film and good textured final YBCO film, but the structure is porous. Heating rate has no significant effect on critical transition temperature (T_c), however critical current density (J_c) was found to be higher for 3 ^{o}C /hr treated sample. The total process time for the optimized TFA-MOD was found to be 28 hrs.

There is significant porosity observed in the final YBCO films. The critical current density, J_c = 1.3MA/cm^2 and T_c = 88.5 K was observed in these films.

A new method, called Nanoparticle process has been developed with idea of fabricating YBCO film by more economical route and at faster processing speed and lower porosity. Comparative XPS analysis was performed on samples fabricated using TFA-MOD, and Nanoparticle methods. It was observed from XPS spectra analysis that in the Nanoparticle process, the calcined film has yttrium and barium ions bonded to oxygen, while in the TFA-MOD process, yttrium and barium ions are still bonded to fluorine, so additional chemical reaction are required to expel fluorine containing gases, thereby resulting in higher porosity in the final film. The fluorine percentage in the calcined film, which is one of the major disadvantages in case of TFA-MOD process, is very minimal in the Nanoparticle process. Hence the problem of HF evolution is not a big concern in Nanoparticle method.

Surface morphology studies were conducted on samples calcined at faster rates in TFA-MOD method and Nanoparticle method. It was realized that in case of TFA-MOD method when the sample was heated at 1 ^{o}C/min to 500 ^{o}C, the film obtained was crumpled, whereas that using Nanoparticle method resulted in a uniform and smooth films.

The Nanoparticle process has successfully fabricated dense, continuous and well textured YBCO thin films. The porosity has been significantly reduced in these films

when compared to that of TFA-MOD processed films. The total processing time (~ 6 hrs) for the fabrication of the precursor film has greatly reduced when compared to that of TFA-MOD process (~ 19 hrs). The T_c of these films was found to be 89 K which is comparable to that of TFA-MOD processed films (88.5 K). Self field critical current densities over 1 MA/cm^2 at 77 K were routinely observed in these Nanoparticle processed films. The best result that has been obtained is 2 MA/cm^2 at 77 K in self-field. It has to be noted that this value of J_c was attained in less than one year of work on Nanoparticle method when compared to that of TFA-MOD method which has taken more than a decade of work to get to this value. Hence, it is believed that the value of J_c could be improved with further optimization of this process.

4.2 FUTURE WORK

- We have successfully synthesized YBCO films with $J_c > 1$MA/cm^2 in thin films. This value could be increased further by optimizing the process variables in this method.
- Films have been successfully fabricated on a single crystal substrate. Next step would be to use this Nanoparticles method to grow YBCO thin films on the metallic substrates.
- Nanoparticles colloidal route can be used to inculcate fluxpinning sites in the YBCO film to increase the electric performance of YBCO thin film in a magnetic field. Initial results on the use of Ceria nanoparticles in TFA-MOD method have shown promising results on the use of nanoparticle route for

imparting flux pining sites. Further studies have to be done in this direction to improve the electrical properties. A new nanoparticle colloid route has to be developed to fabricate the buffer layer, YBCO layer and the flux pinning centers.

REFFERENCES:

[1] R.de Bruyn Ouboter, IEEE Transactions. Magn. Vol. 23 pp. 355, 1983

[2] V.L. Ginzburg, International Journal of Modern Physics B, Vol. 1, Nos. 3 & 4, pp 651-680, 1987.

[3] Rainer Wesche, High Temperature Superconductors: Materials properties, and Applications, Kluwer academic publishers, 1998, pp 2.

[4] Charles P. Poole Jr, Handbook of Superconductivity, Academic press, 2000, pp 53-55.

[5] Charles P. Poole Jr, Timir Datta, Horacio A. Farach, Copper Oxide Superconductors, John Wiley and sons, 1996.

[6] Rainer Wesche, High Temperature Superconductors: Materials properties, and Applications, Kluwer academic publishers, pp 26, 1998.

[7] A. Thomas and P. Sheanen, Introduction to High Temperature superconductivity, Plenum press, I edition,1996

[8] J.G. Bednorz, K.A. Müller, Physica B: Condensed Matter, Vol. 64, pp 189, 1986.

[9] C. Michel, M. Hervieu, M.M Borel, A. Grandin, F. Deslandes, J. Provost, and B. Raveau, Zeitschrift Fur Physik B- Condensed Matter, Vol. 68, pp. 421-423, 1987.

[10] H. Meada, Y. Tanaka, M. Fukutomi, and T. Asano, Japanese Journal of Applied Physics Part 2- letters 27, (2), pp. L209-L210, 1988.

[11] Z.Z Sheng and A.M Hermann, Nature, Vol. 332, pp 138-139, 1988.

[12] A. Schilling, M. Cantoni, J. D. Guo and H.R. Ott, Nature, Vol. 363, pp. 56-58, 1993.

[13] American Superconductor, Second generation HTS wire : An assessment, pp. 7, 2004.

[14] A. Bourdillon, N.X. Tan Bourdillon, High Temperature Superconductors Processing and Science, Academic Press, Inc., 1994.

[15] M. Meada, M. Kadoi and T. Ikeda, Japan Journal of Applied Physics, Vol. 28, pp L1417, 1989.

[16] F. Moon, Introduction to superconductivity, IBC Techinal Service Limiter, 1989.

[17] S. Bungre, R. Meisels, ZX. Shen, AD. Caplin, Nature, pp. 725-727, 1989.

[18] D. Dimos, P. Chaudhari, J. Mannhart, F. Legoues, Physics Review Letters,Vol. 61 pp. 219-222, 1988.

[19] J. L. MacManus-Driscoll, Annual Review of Material Science, 28, pp. 421-462, 1998.

[20] Y. Iijima, N. Tanabe, O. Kohno, and Y. Ikeno, Applied Physics Letters, Vol. 60, pp. 769-771, 1992.

[21] B. Ma, M. Li, Y. A. Jee, R.E. Koritala, B.L. Fisher, U. Balachandran, Physica C, Vol. 366, pp. 270-276, 2002.

[22] D.P. Norton, Annual Review of Material Science, Vol. 28, pp 299-243, 1998

[23] P.N. Arendt, IEEE Transactions on Applied Superconductivity, Vol. 4, pp. 429-434, 1998.

[24] A. Usoskin, F. Garcia-Moreno, J. Knoke, S. Sievers, J. Dzick, and H.C. Freyhardt, IOP, Inst. Phys. Conf: Ser., no.167, vol. 1, pp. 447-450, 1999.

[25] A. Sheth, H. Schmidt, V. Lasrado, Applied Superconductivity, 6, 10-12, pp. 855-873, 1998.

[26] S. R. Foltyn, P. Tiwari, C. Dye, M. Q. Le, and X.D. Wu, Applied physics letters, Vol. 63, pp. 1848, 1993.

[27] Y. Iijima, K. Matsumoto, Superconductor Science and Technology, Vol. 13, pp. 68, 2000.

[28] A. Usoskin and H. C. Freyhardt, MRS Bulletin, Vol. 29, 8, pp. 583- 589, 2004.

[29] K. Onabe, S. Nagaya, T. Shimonosono, Y. Iijima, N. Sadakata, T. Saito, O. Kohno, Proceedings 16th intl. Cryogenic Engineering conference/ Int. Cryogenic Materials Conference., edited T. Haruyama, T. Mitsui, K. Yamafuji, Oxford ,UK: Elsevier Science, pp.1413, 1997 ,.

[30] V. Selvamanikam, G. Carota, M. Funk, N. Vo, P. Haldar, U. Balachandran, M. Chudzik, P. Arendt, J.R Groves, R. DePaula, B. Newman, IEEE transactions Applied Superconductivity, Vol. 11, pp. 3379, 2001.

[31] J. Qiao, C.Y. Yang, Materials Science and Engineering, R 14, pp. 157 – 202, 1995.

[32] P. Chou, Q. Zhong, Q.L. Li, K. Abazajian, A. Ignatiev, C.Y. Wang, E.E. Deal, J.G. Chen, Physica C, 1997 ,Vol. 254, pp. 93, 1995.

[33] F. Parmigaini, G. Chiarello, N. Ripamonti, H. Fotezki, U. Rollu, Physics Review Letters B, Vol. 36, pp. 7148, 1987.

[34] A. Gupta, R. Jaganathan, E.I. Cooper, E.A. Giess, J.I. Lanman, B.W. Hussey, Applied Physics Letters, Vol. 52, pp. 2077, 1988 .

[35] P.C. McIntyre, M.J. Cima, M.F. Ng, Journal of Applied Physics, Vol. 68, pp. 4183, 1990.

[36] T. Araki, K. Yamagiwa, I. Hirabayashi, Cryogenics, Vol. 41, pp. 675, 2001.

[37] J.H. Su, P. P. Joshi, V. Chintamaneni, S. M. Mukhopadhyay, Superconductor Science and Technology, Vol. 18, pp. 1496, 2005.

[38] P. M. Mankiewich, J.H. Scofield, W.J. Skocpol, R.E. Howard, A.H. Dayem, and E. Good, Applied Physics Letters, Vol. 51, pp. 1753-1755, 1987.

[39] Y.A. Jee, B. Ma, V.A. Maroni, M. Li, B.L. Fisher, U. Balachandran, Superconductor Science Technology, Vol. 14, pp. 285, 2001.

[40] D. H. Liebenberg, P. C. McIntyre, M.J. Cima, T.A. Francavilla, Cryogenics, Vol. 32, pp. 1066, 1993

[41] M.P. Siegal, J.T. Dawley, P.G. Clem, and D.L. Overmyer, Physica C, Vol. 399, pp. 143, 2003.

[42] T. Araki, H. Kurosaki, Y. Yamada, I. Hirabayashi, J. Shibata, T Hirayama, Superconductor Science and Technology, Vol. 14, pp. 783, 2001.

[43] T. Araki, H. Kurosaki, J. Shibata, T. Hirayama, I. Hirabayashi, Superconductor Science and Technology, Vol. 14, pp. 783, 2001.

[44] J.A. Smith, M.J. Cima, N. Sonnenberg, IEEE Transactions Applied Superconductivity, Vol. 9, pp. 1531, 1999.

[45] J.T. Dawley, P.G. Clem, T.J. Boyle, L.M. Ottley, D.L. Overmyer, M.P. Siegal, Physica C, Vol. 402, pp. 143, 2004

[46] T. Araki, I. Hirabayashi, J. Shibata, Y. Ikuhara, Superconductor Science and Technology, Vol. 15, pp. 913-916, 2002

[47] P.C. McIntyre M.J. Cima, Journal of Materials Research, Vol. 9, pp. 2778,1994

[48] Y. Tokunaga et al., Physica C, Vol. 412-414, pp. 910, 2004

[49] C.D. Wagner, W.M. Riggs, L.E. Davis, J.F. Moulder, and G.E. Muilenberg, Handbook of X-ray Photoelectron Spectroscopy, Perkin-Elmer, Eden Prairie, MN, 1979

[50] John B. Wachtman, Charaterization of Materials, Mannning Publications Co, CT, 1993

[51] R.P. Vasquez, M.C. Foote, and B.D. Hunt, Journal of Applied Physics, Vol. 66, pp. 4866, 1989.

[52] G.E. Murch, R.J. Thorn, Journal of Physics Chemistry of Solids, Vol. 41, pp. 785, 1980.

[53] J.C. Klein, P.L. Chung, D.M. Hercules, J.F. Black, Applied Spectroscopy, Vol. 38 pp. 729, 1984.

[54] Y. Uwamino, A. Tsuge, T. Ishizuka, H. Yamatera, Bulletin of Chemical Society Japan, Vol. 59, pp. 2263, 1986.

[55] M. Rizhkov, V.A. Gubanov, M.P. Bytzman, A.L. Hagström, E.Z. Kurmaev, Journal of Electron Spectroscopy and Related Phenomenon, Vol.18, pp.227, 1980.

[56] J. Santiso, A. Figueras, A. Moya, F. Baudenbacher, Physica C, Vol. 351, pp.155, 1991.

[57] Y. Pan, J.H. Zhu, M.H. Hu, E.A. Payzant, Surface Coatings and Technology, Vol. 200, pp. 1242 – 1247, 2005.